Engineering an Exo70 integrated domain of a barley NLR for improved blast resistance

Indira Saado[1], Helen J. Brabham[2,3], Josh W. Bennett[1], Anson Ho Ching Lam[4], Inmaculada Hernández-Pinzón[2], Matthew J. Moscou[2,5], Juan Carlos De la Concepcion[1,2,6*], Mark J. Banfield[1*]

Address:

[1] *Department of Biochemistry and Metabolism, John Innes Centre, Norwich Research Park, Norwich, NR4 7UH, UK*

[2] *The Sainsbury Laboratory, University of East Anglia, Norwich Research Park, Norwich, NR4 7UH, UK*

[3] *2Blades, Evanston, IL 60201, USA*

[4] *Department of Cell and Developmental Biology, John Innes Centre, Norwich Research Park, Norwich, NR4 7UH UK*

[5] *USDA-ARS Cereal Disease Laboratory, University of Minnesota, 1551 Lindig Street, Saint Paul, Minnesota, 55108 USA*

[6] *Gregor Mendel Institute of Molecular Plant Biology, Austrian Academy of Sciences, Vienna, 1030, Austria*

[*]Corresponding authors: Juan Carlos De la Concepcion (juan.concepcion@gmi.oeaw.ac.at), Mark J. Banfield (mark.banfield@jic.ac.uk)

ORCID IDs:

Indira Saado: 0000-0002-3462-0983

Helen Brabham: 0000-0001-7132-5011

Josh W. Bennett: 0000-0001-8576-7195

Anson Ho Ching Lam: 0000-0001-7805-2132

Inmaculada Hernández-Pinzón: 0000-0003-3711-2893

Matthew J. Moscou: 0000-0003-2098-6818

Juan Carlos De la Concepcion: 0000-0002-7642-8375

Mark J. Banfield: 0000-0001-8921-3835

Summary

Intracellular immune receptors protect plants from microbial invasion by detecting and responding to pathogen-derived effector molecules, often triggering cell death responses. However, pathogen effectors can evolve to avoid immune recognition, resulting in devastating diseases that threaten global agriculture. Here, we show that an integrated Exo70 domain from the barley NLR RGH2 can interact with both the rice blast pathogen effector AVR-Pii and a closely related wheat blast variant. We used structure-led engineering to develop RGH2^{+} that shows increased binding affinity towards AVR-Pii variants and increased cell death responses on heterologous expression in *Nicotiana benthamiana*. Infection assays in transgenic barley lines harbouring RGH2^{+} (along with the paired NLR RGH3) show reduced virulence towards blast strains expressing AVR-Pii variants. These results demonstrate the potential of engineering NLR receptors as an effective strategy for improving resistance towards one of the most destructive diseases affecting cereal production.

Introduction

Plants are continuously threatened by pathogens and rely on an innate immune system for defence. One critical component of this immune system is the recognition of virulence proteins (effectors) that are delivered from pathogens to manipulate host cells for the benefit of the invading organism. *Magnaporthe oryzae* is a devastating ascomycete fungus that infects cereal crops, including rice, wheat, barley, and other grasses, causing blast disease[1,2]. Since the pathogen's host jump to wheat in South America in the 1980s[3,4], and recent spread to Asia and Africa[5], wheat blast disease (caused by *M. oryzae* pathotype *triticum*) has emerged as major pandemic threat to agriculture. *M. oryzae* deploys a diverse set of effectors during colonization, targeting key plant processes to promote infection. Despite their essential roles in infection, the function of only a limited number of *M. oryzae* effectors has been fully characterized.

As well as promoting infection, effectors can be sensed by intracellular nucleotide-binding leucine-rich repeat (NLR) receptors, triggering immune responses that often result in localised cell death, limiting the spread of infection. As such, engineering NLRs for novel recognition profiles can unlock promising strategies for improved disease resistance[6–9]. Canonical NLRs comprise an N-terminal signalling domain, a central nucleotide-binding adaptor NB-ARC switch domain, and a C-terminal leucine-rich repeat (LRR) domain involved in intramolecular molecular contacts and pathogen effector recognition[10]. While some NLRs function alone to both sense and respond to effectors (singleton NLRs), others function in pairs, with a sensor NLR to recognize the effector, directly or indirectly, and a helper NLR required for immune response execution. Such pairs can be co-located in plant genomes (including in head-to-head orientations with shared promoters), or function as part of distributed genetic networks[11,12].

To date, two co-located paired NLR systems have been extensively studied in rice: Pik-1/Pik-2[13,14] and RGA5/4[15,16]. Both sensor NLRs, Pik-1 and RGA5, contain non-canonical integrated heavy metal-associated (HMA) domains to bait specific effectors from *M. oryzae*[17–20]. The sensor NLR Pik-1 contains a HMA domain positioned between the CC and NB-ARC domains, and with the helper NLR Pik-2 cooperatively triggers immunity against the blast pathogen effector AVR-Pik[13,14,18,21,22]. The Pik/AVR-Pik system has emerged as a model for how receptor engineering can lead to novel

immune outcomes[6–8,19,20,23,24]. By contrast, the sensor NLR RGA5 has an HMA domain at the C-terminus (after the LRR) and baits the blast pathogen effectors AVR-Pia and AVR1-CO39[25]. Activation of immunity requires the helper NLR RGA4[26,27]. This NLR pair has also been leveraged for engineering immunity to expand effector recognition profiles[28].

In addition to direct effector recognition, paired NLRs can indirectly recognise pathogen effectors[29–31]. For example, the unconventional RIN4 (RPM1-Interacting Protein 4)-like NOI (nitrate induced) domain of the rice sensor NLR Pii-2 monitors the status of host OsExo70-F2/3 proteins targeted by the rice blast Zinc-finger fold (ZiF) effector AVR-Pii[29–32]. Canonical Exo70 proteins are part of the exocyst, a conserved protein complex essential for tethering secretory vesicles to membranes[33,34].However, in plants, the Exo70 family has dramatically expanded[35] and acquired novel functions independent from the exocyst[33,36–38], including plant defence[39–43], making this protein a target for pathogen effectors[44]. Integrated domains in NLRs, such as HMAs, are likely derived from the host virulence-associated targets of effectors, repurposed for effector perception[45]. Recently, a head-to-head NLR pair from the barley cultivar Baronesse was identified comprising the sensor NLR RGH2, containing a C-terminal Exo70 integrated domain, and its helper NLR RGH3[46]. The integration of an Exo70 domain in RGH2[47] suggests a potential role in immunity by serving as an integrated domain to bait effectors for recognition.

In this study, we show that the Exo70 integrated domain of the barley sensor NLR RGH2 can interact with the rice blast effector AVR-Pii and a closely related wheat blast variant in vitro and in vivo. On co-expression with the helper NLR RGH3, the RGH2/RGH3 pair elicits limited cell death to the AVR-Pii variants in *N. benthamiana*. However, transgenic barley expressing RGH2/RGH3 are susceptible to *M. oryzae* strains expressing AVR-Pii variants. Based on the crystal structure of the OsExo70F2/AVR-Pii complex[29], we engineered a new immune receptor, RGH2^{+}, that showed enhanced binding affinity towards both AVR-Pii variants, leading to improved cell death responses on co-expression with RGH3 in *N. benthamiana*, and a reduction in disease severity in transgenic RGH2^{+}/RGH3 barley plants challenged with *M. oryzae* strains harbouring AVR-Pii variants. These findings establish the RGH2/RGH3 NLR pair as a platform for engineering enhanced effector response profiles and highlights new opportunities for protecting cereal crops from blast disease.

Results

Multiple Exo70 domains are integrated across the Poales order

Previous work established that NLRs from diverse plant species carry integrated domains[48,49]. We sought to identify NLRs with integrated Exo70 domains to understand their source and assess their use as scaffolds for NLR engineering. To enrich the set of NLRs for analysis, we performed de novo transcriptome assembly of publicly available RNAseq data for 102 Poales species including a total of 292 accessions (Figure 1A). Domain annotation identified 184,775 NB-ARC domain containing proteins. Within this set of NB-ARC containing proteins, 82 were found to also have an Exo70 domain. Comparative analysis of these integrated Exo70 domains found that the 82 putative integrated Exo70 domains are derived from eight unique fusion events. Among these, six domains were found to be of sufficient length for phylogenetic analysis with grass Exo70 domains[43]. Maximum likelihood phylogenetic analysis using Exo70 from eight grass species found the six integrated Exo70 domains were placed in either the Exo70F or Exo70FX clades (Figure 1B). The most prevalent integration is RGH2 that carries a C-terminal fusion with Exo70F1, which was originally identified at the *Mla* locus in the barley (*Hordeum vulgare*) accession Baronesse. This integration event was found in seven species within Triticeae and Poeae tribes[47]. In barley, a second NLR, Hvu23934, was found with integration of Exo70FX2 in three Triticeae species (*Aegilops sharonensis*, *Ae. speltoides*, and *H. vulgare*). The remaining four integrated domains are found in single species: *Arundinella pubescens* (Panicoideae; Apu26724; NLR-Exo70F4), *A. pubescens* (Panicoideae; Apu28443; NLR-Exo70F2), *Holcus lanatus* (Pooideae; Hla80948; NLR-Exo70FX2), and *Juncus effusus* (Juncaceae; Jef9120; NLR-Exo70F), Figure S1. Five of these NLRs were taken forward for further analysis (excluding Apu26724).

Rice blast AVR-Pii and the wheat blast variant bind the barley RGH2-Exo70 integrated domain in yeast

As some ZiF effectors, including AVR-Pii, bind rice Exo70s from clade F, we tested whether Exo70 integrated domains could bind ZiF effectors from rice and wheat-infecting blast isolates of *M. oryzae* in pairwise yeast two-hybrid (Y2H) assays. For this we cloned the Exo70 integrated domains from the NLRs RGH2, Hvu23924, Hla80948, Jef9120, and Apu28443 and tested their binding to representatives of each ZiF effector clade from rice and wheat-infecting blast isolates. These assays revealed

144 that ZiF effectors from clade VIII, from both rice blast (ZiF_VIIId, hereafter AVR-Pii^{Rb})
145 and wheat blast (ZiF_VIIIc, hereafter AVR-Pii^{Wb}) isolates bound RGH2-Exo70, as did
146 clade IX member ZiF_IXj (Figure 2A). We did not observe interactions between other
147 NLR Exo70 integrated domains and any ZiF effectors tested (Figure S3A, S4A, S5A).
148 We observed yeast growth with Apu28443-Exo70 in the presence of all tested ZiF
149 effectors, indicating likely artefactual autoactivity (Figure S6A). Therefore, we did not
150 investigate it further in this study. Protein accumulation was assessed by western blot
151 (Figure S2A, S3B, S4B, S5B, S6B).

152 The crystal structure of AVR-Pii^{Rb} in complex with OsExo70F2[29] identified Phe-65 as
153 a key interacting residue from the effector, and a Phe65Glu mutation in AVR-Pii^{Rb}
154 abolished the interaction with OsExo70F3[29]. AVR-Pii^{Wb} is predicted to adopt the
155 conserved ZiF structural fold, as observed for AVR-Pii^{Rb} (Figure S7A, B), and binds to
156 OsExo70F3[32]. To test whether AVR-Pii^{Rb} and AVR-Pii^{Wb} interact with the RGH2-Exo70
157 integrated domain via a similar interface, we tested the binding of both AVR-Pii^{Rb} and
158 AVR-Pii^{Wb} Phe to Glu mutants to RGH2-Exo70 by Y2H. This assay revealed that these
159 mutants do not bind RGH2-Exo70 (Figure 2B). Protein accumulation was assessed by
160 western blot (Figure S2B).

161 AVR-Pii^{Rb} and AVR-Pii^{Wb} bind the barley RGH2-Exo70 integrated domain 162 in planta

163 To further validate the interaction between AVR-Pii^{Rb} or AVR-Pii^{Wb} with RGH2-Exo70,
164 we used co-immunoprecipitation (co-IP) assays in *N. benthamiana*. RGH2-Exo70-
165 FLAG was co-expressed with GFP-AVR-Pii^{Rb}, GFP-AVR-Pii^{Wb} and their respective
166 Phe to Glu mutants. We also co-expressed the effectors with OsExo70F3-FLAG as
167 positive and negative controls, respectively. Following extraction and
168 immunoprecipitation with anti-FLAG beads (to capture Exo70 domains), both
169 effectors, but not their Phe to Glu mutants, were pulled down (Figure 2C). Interestingly,
170 we observe that the qualitative levels of AVR-Pii^{Rb} and AVR-Pii^{Wb} in the co-IPs are
171 higher with OsExo70F3 compared to the RGH2-Exo70, suggestive of a stronger
172 association.

173

AVR-Pii^{Rb} and AVR-Pii^{Wb} bind more weakly to RGH2-Exo70 than OsExo70F3 in vitro

To further investigate the binding of AVR-Pii^{Rb} and AVR-Pii^{Wb} to RGH2-Exo70 we produced and purified these proteins in *Escherichia coli*. We then performed isothermal titration calorimetry (ITC) assays to assess the binding strength between effectors and the RGH2-Exo70 domain. Previous results show that AVR-Pii^{Rb} binds to OsExo70F3 in the nano-molar range (K_D of 1.0x10^{-10} M)[29]. RGH2-Exo70 binds AVR-Pii^{Rb} and AVR-Pii^{Wb} in the micro-molar range (K_Ds of 1.5x10^{-5} M and 6.7x10^{-6} M respectively), showing that AVR-Pii^{Rb} bind OsExo70F3 more tightly than RGH2-Exo70 in vitro (Figure 2D), and AVR-Pii^{Wb} binds RGH2-Exo70 in the same range as AVR-Pii^{Rb}. No binding was observed with the effector mutants AVR-Pii^{RbF65E} or AVR-Pii^{WbF65E} with OsExo70F3 or RGH2-Exo70 (Figure 2D)[29].

Taken together, the results from Y2H, co-IP, and ITC show that while AVR-Pii^{Rb} and AVR-Pii^{Wb} bind to RGH2-Exo70, this interaction is not as robust as to OsExo70F3. This suggests that engineering RGH2-Exo70 for improved effector binding could enhance effector perception and immunity-related signalling by this receptor.

An engineered RGH2^{+} NLR shows higher binding affinity towards AVR-Pii^{Rb} and AVR-Pii^{Wb}

We hypothesised that engineering a new binding interface to RGH2-Exo70, mimicking OsExo70F3, could improve interaction strength. Guided by the structure of the OsExo70F2/AVR-Pii complex[29], we generated a modified version of RGH2, RGH2^{+}, by introducing three mutations, Ala1378Val, Ile1379Leu, and Leu1396Met (Figure 3A). AlphaFold3[50] predictions of the RGH2-Exo70 and RGH2^{+}-Exo70 structures indicate a conserved fold with OsExo70F2 (Figure 3B).

To assess the binding capabilities of the RGH2^{+}-Exo70 domain towards AVR-Pii^{Rb} and AVR-Pii^{Wb} we first used the Y2H assay. This showed that the engineered NLR retained binding to these two effectors, and confirmed the same surface of the effector is required for binding as the respective Phe to Glu mutations prevented interaction (Figure 3C). Protein accumulation was assessed by western blot (Figure S8).

To compare interactions between AVR-Pii^{Rb} and AVR-Pii^{Wb} with RGH2 or RGH2^{+} in plant cells, we first used co-IP. FLAG-tagged full-length RGH2 and RGH2^{+}

205 immunoprecipitated GFP-tagged AVR-Pii^{Rb} and AVR-Pii^{Wb}, but not the AVR-Pii^{F65E}
206 mutants of each effector (Figure 3D). Additional negative controls, including a double
207 mutant AVR-Pii$^{Y64A/F65E}$ and a ZiF effector from a clade that does not interact with
208 Exo70s (ZiF_IIb), were not immunoprecipitated by RGH2 or RGH2^{+} (Figure S9).
209 Secondly, we used the split GAL4 RUBY assay that allows quantification of protein-
210 protein interactions in plant cells through the production of betalain[51]. Agrobacterium
211 carrying OsExo70F3-Gal4-BD, RGH2-Exo70-Gal4-BD, or RGH2^{+}-Exo70-Gal4-BD
212 were co-infiltrated with constructs containing VP16-tagged rice blast AVR-Pii and the
213 wheat blast variant or their Phe to Glu mutants (all constructs under the control of the
214 *35Sprom*). Betalain production was observed 3 days post-infiltration (dpi) (Figure
215 S10A, S11A). Intriguingly, significantly higher betalain production was observed in
216 RGH2^{+}-Exo70 leaves compared to RGH2-Exo70 with AVR-Pii^{Rb}. However, with VP16-
217 AVR-Pii^{Wb}, levels of betalain production accumulated at similar levels. Low betalain
218 production was observed with the VP16-tagged effector mutants in combination with
219 Exo70 constructs. To determine whether lower effector expression in *N. benthamiana*
220 leaves could allow distinction between RGH2-Exo70 and RGH2^{+}-Exo70 responses to
221 AVR-Pii^{Wb} in this assay, we generated AVR-Pii expression constructs under the control
222 of the *MAS* promoter. Notably, overall betalain production was lower compared to the
223 *35Sprom* assays. However, in these conditions, we observed significant differences
224 between RGH2-Exo70 and RGH2^{+}-Exo70 with both AVR-Pii^{Rb} and AVR-Pii^{Wb} (Figure
225 4A, B). Protein accumulation for all constructs was assessed by western blot (Figure
226 S10B, S11B).

227 RGH2^{+}-Exo70 binds AVR-Pii^{Rb} and AVR-Pii^{Wb} more tightly compared to 228 wild-type in vitro

229 To extend the in vivo analysis, we purified RGH2^{+}-Exo70 from *E. coli* and tested
230 binding to AVR-Pii^{Rb} and AVR-Pii^{Wb} by ITC. Consistent with the RUBY assay, the
231 binding affinity of RGH2^{+}-Exo70 to AVR-Pii^{Rb} and AVR-Pii^{Wb} was increased compared
232 to RGH2-Exo70, with a dissociation constant (K_D) of 3.12×10^{-6} M and 1.06×10^{-6} M,
233 respectively (Figure 4C). No binding to RGH2^{+}-Exo70 was observed with AVR-Pii^{RbF65E}
234 or AVR-Pii^{WbF66E} (Figure 4C). These in vitro experiments confirmed tighter binding of
235 RGH2^{+}-Exo70 towards AVR-Pii^{Rb} and AVR-Pii^{Wb} compared to the wild type RGH2-
236 Exo70, as observed in planta.

RGH2^{+}/RGH3 enhanced cell death responses to AVR-Pii^{Rb} and AVR-Pii^{Wb} in *N. benthamiana*

We hypothesised that increased effector binding to RGH2^{+}-Exo70 may translate into improved immune responses in plants compared to RGH2. To test this, we first co-expressed RGH2 and RGH3 in *N. benthamiana* alone to assess potential autoactivity, and with AVR-Pii^{Rb} or AVR-Pii^{Wb} to observe effector-dependent cell death. Imaging leaves three days post infiltration revealed that no macroscopic cell death was observed for RGH2/RGH3 alone, or when co-expressed with GFP or with effector Phe to Glu mutants (Figure 5A, 5B). However, cell death was observed under both white light and UV light on co-expression of RGH2/RGH3 and either of AVR-Pii^{Rb} or AVR-Pii^{Wb} (Figure 5A, 5B). In parallel, to test the impact of RGH2^{+} on cell death, we co-expressed this NLR with RGH3, both with and without effectors. Again, we did not observe autoactivity, or cell death with negative controls. Intriguingly, we observed qualitatively stronger cell death in leaf spots infiltrated with RGH2^{+} compared to RGH2, and the cell death was stronger with AVR-Pii^{Wb} over AVR-Pii^{Rb} (Figure 5A, 5B). To quantify the cell death on expression of NLRs and effectors in *N. benthamiana*, we measured electrolyte leakage from leaf disks at 4, 24, and 48 hours post-infiltration (Figure 5C, S12A, B). Here, we observed significant increases in conductivity from samples of RGH2^{+}/RGH3-infiltrated tissue with AVR-Pii^{Wb} over AVR-Pii^{Rb} compared to RGH2/RGH3. RGH2/RGH3 or RGH2^{+}/RGH3 with AVR-Pii^{F65E} displayed minimal change in conductivity compared with RGH2/RGH3 and RGH2^{+}/RGH3 alone (Figure 5C, Figure S12A, B). We also observed higher levels of conductivity in samples with AVR-Pii^{Wb} compared to AVR-Pii^{Rb}, in agreement with the macroscopic cell death observations. Protein accumulation was assessed by western blot for all *N. benthamiana* cell death experiments (Figure 5D, E). Collectively, these data demonstrate that RGH2^{+}/RGH3 exhibits a stronger cell death response towards the effectors compared to RGH2/RGH3 in *N. benthamiana*, and that AVR-Pii^{Wb} elicits a stronger response than AVR-Pii^{Rb}.

Enhanced recognition of AVR-Pii^{Wb} by RGH2^{+}/RGH3 in transgenic barley plants

We hypothesised that the increase in cell death response of RGH2^{+}/RGH3 to effectors compared with RGH2/RGH3 in *N. benthamiana*, could improve the response of barley

269 to pathogens encoding these effectors. For this, we focussed on AVR-Pii^{Wb} due to the
270 need to explore novel resistances against wheat blast[52].

271 RGH2/RGH3 was previously cloned with the native promoter and terminator and
272 transformed into the barley cultivar Golden Promise[46]. The RGH2/RGH3 genomic
273 transformation construct was edited using site-directed mutagenesis to covert the
274 integrated Exo70 binding site into RGH2+ and was transformed into the barley cultivar
275 Golden Promise using Agrobacterium-mediated transformation.

276 RGH2^{+}/RGH3 and RGH2/RGH3 transgenic Golden Promise T1 families were tested
277 for recognition of AVR-Pii^{Wb} by inoculation with *M. oryzae* isolate Sasa2 (wild-type
278 virulent on Golden Promise) transformed with AVR-Pii^{Wb} using a spray-based
279 inoculation. For RGH2, a total of 82 individuals from across 5 independent T1 families
280 were screened in replicate 1 and a total of 85 individuals from across 5 independent
281 T1 families in replicate 2. For RGH2^{+}, a total of 97 individuals from across 4
282 independent T1 families were screened in replicate 1 and a total of 99 individuals from
283 across 4 independent T1 families were screened in replicate 2. Phenotypes were
284 assessed on a macroscopic semi-quantitative scale for disease severity[53]. We
285 observed a significant difference in growth of Sasa2 + AVR-Pii^{Wb} on RGH2^{+} compared
286 with RGH2 transgenics (Figure 6A, C).

287 For further quantitative comparison, RGH2 and RGH2^{+} transgenics were inoculated
288 with *M. oryzae* isolates BTJP 4-1 (containing AVR-Pii^{Wb}), Sasa2 wild-type, and Sasa2
289 + AVR-Pii^{Wb}. Each isolate was used for spot inoculations on the same barley leaf and
290 evaluated by measuring individual lesion sizes. For RGH2 transgenics, a total of 101
291 individuals from across 8 independent T1 families were screened in replicate 1 and a
292 total of 92 individuals from across 6 independent T1 families were screened in replicate
293 2. For RGH2^{+} transgenics, a total of 47 individuals from across 3 independent T1
294 families were screened in replicate 1 and a total of 98 individuals from across 4
295 independent T1 families were screened in replicate 2. Lesion sizes were significantly
296 reduced in RGH2^{+} plants inoculated with BTJP 4-1 compared to RGH2 and with one
297 replicate of Sasa2 + AVR-Pii^{Wb} (Figure 6B, D).

298 To assess heritability of resistance, T2 families of RGH2 and RGH2^{+} transgenics were
299 inoculated with all three isolates using a spot inoculation. For RGH2, a total of 107
300 individuals from across 5 independent T1 families were screened in replicate 1 and a

301 total of 21 individuals from across 5 independent T1 families in replicate 2. For RGH2^{+},
302 a total of 61 individuals from across 4 independent T1 families were screened in
303 replicate 1 and a total of 30 individuals from across 4 independent T1 families were
304 screened in replicate 2. A significant difference was observed between RGH2^{+} and
305 RGH2 families in one replicate for Sasa2 + AVR-Pii^{Wb} (Figure S13). Variation in lesion
306 sizes and phenotypic differences were observed across replicates and the power of
307 statistical analyses may have been reduced due to variation in isolate virulence.
308 Comparing across all inoculations, RGH2^{+}/RGH3 confers a small but significant
309 reduction in disease lesions with Sasa2 + AVR-Pii^{Wb} and BTJP 4-1 compared to Sasa2
310 wild-type.

311

312 ## Discussion

313 NLR immune receptors play a crucial role in protecting plants against pathogens and
314 are a critical component of disease resistance breeding programs in crops. The
315 diverse effector repertoires of pathogens and their ability to adapt to immune systems
316 presents challenges that can limit the effectiveness of NLRs deployed in agriculture.
317 Approaches to address this limitation include engineering NLRs to broaden their
318 recognition spectrum to target conserved effectors across pathogen isolates. Here, we
319 have introduced structure-guided mutations in the effector binding interface of the
320 Exo70 integrated domain of the barley NLR immune receptor RGH2 to enhance
321 binding to rice and wheat blast effectors. Using a combination of in vitro and in vivo
322 experiments, we demonstrate this engineered RGH2^{+} shows higher affinity binding
323 towards rice blast AVR-Pii and the wheat blast variant compared to RGH2, leading to
324 improved immune responses and reduced pathogen virulence in transgenic barley
325 lines.

326 With the emergence of new disease pandemics, such as wheat blast that threatens
327 yields across Asia and Africa, there is a pressing need for identifying new sources of
328 resistance[54–56]. Screening wild species and landraces for novel resistance traits
329 continues to deliver new genes and germplasm for breeding[57]. Alternative approaches
330 are enabled by advances in understanding the molecular mechanisms of plant
331 immune receptor structure and function. Such knowledge can be deployed through
332 engineering and improved transformation pipelines, alongside ongoing improvements
333 in gene-editing tools.

334 NLR integrated domains (NLR-IDs) bait pathogen effectors for immune activation in
335 cereals and other plants[14,58–60]. They present opportunities for receptor engineering,
336 to optimise effector recognition ahead of activating conserved downstream
337 mechanisms of NLR-mediated immunity[14,59]. Exo70 integrated domains are under-
338 studied compared to other examples such as HMA and WRKY domains[13,14,16,20,59,60].
339 The best studied example of NLR-mediated immunity requiring Exo70 proteins is
340 towards the *M. oryzae* effector AVR-Pii. However, in this case the Exo70 protein is
341 guarded by the NLR pair Pii, and not integrated within an immune receptor[30,31]. In
342 plants, Exo70 proteins form an expanded family with increased gene copy number
343 and functional diversification[35,36,38,43] and they are targeted by effectors from diverse

344 pathogens[44]. Here, our studies highlight the potential of engineering NLR integrated
345 Exo70 domains to mediate activation of immunity.

346 Our rationale for RGH2-Exo70 engineering was guided by the interface formed in the
347 crystal structure of the OsExo70F2/AVR-Pii complex[29]. The mutations to generate
348 RGH2^{+} resulted in subtle changes to amino acid properties at the interface, including
349 Alanine to Valine (position 1378), Isoleucine to Leucine (position 1379) and Leucine
350 to Methionine (position 1396). We hypothesised these differences could explain the
351 reduced affinities of AVR-Pii^{Rb} and AVR-Pii^{Wb} to RGH2-Exo70 over OsExo70F3, and
352 ultimately improve the binding and response of the RGH2^{+}/RGH3 pair. Subtle changes
353 acquired in effectors through evolution can result in escape from detection by plant
354 immune receptors, potentially reducing their effectiveness in crops. By contrast, we
355 show here that subtle amino acid changes can be harnessed to engineer receptors to
356 boost plant immunity, including to effector families conserved across pathogen
357 isolates. However, while OsExo70F3 binds AVR-Pii^{Rb} with nanomolar affinity, RGH2^{+}
358 binding to AVR-Pii^{Rb} and AVR-Pii^{Wb} remains within the micromolar range. This
359 suggests there may be opportunities, beyond the scope of this study, to further improve
360 effector binding to RGH2 and response to wheat blast expressing AVR-Pii^{Wb}.

361 Effectors form diverse sequence and structural repertoires across different pathogen
362 isolates[61–63]. AVR-Pii^{Rb} and AVR-Pii^{Wb} are both members of tribe VIII of the Zinc-finger
363 (ZiF) effector family[32], sharing 72 % sequence identity. We observed that AVR-Pii^{Rb}
364 and AVR-Pii^{Wb} elicit different levels of RGH2/RGH3 activation, which was even clearer
365 with RGH2^{+}/RGH3. Specifically, AVR-Pii^{Wb} more strongly elicited cell death compared
366 to AVR-Pii^{Rb} in *N. benthamiana* assays (Figure 5A). ZiF effectors from different tribes
367 (including tribe VIII) are prevalent in wheat blast lineages compared to rice blast,
368 where many are either absent or are pseudogenes[32]. While we focussed on
369 engineering the barley NLR RGH2 receptor pair towards AVR-Pii^{Rb} and AVR-Pii^{Wb}
370 here, there are future opportunities to expand responses towards other ZiF family
371 members by exploring surface complementarity between predicted effector structures
372 and the binding sites of Exo70 integrated domains using computational approaches[64].
373 In particular, this includes members from ZiF effector Tribes VII and IX, as these were
374 previously shown to bind OsExo70F3[32].

375 In this study, we aimed to engineer new resistance to effectors from the blast pathogen
376 (specifically wheat blast) and in general broaden our understanding of NLR-mediated
377 resistance mechanisms. Engineering of the barley RGH2 guided by the binding of rice
378 blast AVR-Pii to OsExo70F2 successfully conferred reduced virulence to *M. oryzae*
379 when introduced in transgenic barley. Additional work, possibly through additional
380 increases in receptor-effector binding or by investigating NLR expression levels in
381 transgenic plants, is required to further optimise the reduced virulence conferred by
382 RGH2+/RGH3 against wheat blast.

383 ## Conclusion and outlook

384 Engineering NLR integrated domains is a promising path to expand the effector
385 recognition profile of these plant immune receptors. Previously, the rice NLR pairs Pik
386 (Pik-1/Pik-2) and Pia (RGA4/RGA5), which both contain integrated HMA domains in
387 their sensor NLRs to bait effectors, have been engineered with novel response profiles
388 [19,20,28,65]. Here, we further the concept of NLR integrated domain engineering to the
389 Exo70 domain of the RGH2/RGH3 pair, demonstrating its promise as a scaffold to
390 expand the spectrum of effector recognition specificities.

391 Looking ahead, future directions could involve applying this system to wheat cultivars.
392 Interestingly, RGH2/RGH3 is present in rice, however RGH2 has an integrated
393 thioredoxin domain rather the Exo70[47]. As AVR-Pii has been lost from most *M. oryzae*
394 isolates infecting rice (likely due to deployment of Pii-based resistance in rice) the
395 evolution of different integrated domains in the RGH2/RGH3 architecture supports this
396 chassis as an appropriate target for engineering. Finally, it may be possible to engineer
397 resistance to other pathogens by installing additional diverse Exo70 domains, or other
398 unrelated effector targets.

399 # STAR Methods

400 ## Plasmids and cloning procedures

401 *Escherichia coli* Stellar™ (Takara Bio), SHuffle (Invitrogen) and Rosetta™ (DE3) cells
402 were used for cloning and protein expression. All plasmids were generated by either
403 In-fusion cloning (Takara Bio, USA) or the Goldengate system[66] using resources from
404 TSL Synbio. All plasmids are described in Supplemental Table S1, enabling full details
405 of constructs used, including epitope tags. The modules used were either amplified by
406 PCR, synthesized as PCR products (Gblocks, GeneWiz) or obtained from TSL SynBio.
407 Restriction enzymes were purchased from New England Biolabs (Ipswich, MA, USA).
408 Primers and their purpose are listed in Supplemental Table S2.

409 ## Experimental model and subject detail

410 **Nicotiana benthamiana**

411 *Nicotiana benthamiana* plants were grown in controlled long-day conditions (16-h light
412 (in combination of 2 Philips ter TL-D 58W/840 and Sylvania GRO-LUX F58W/GRO-T8
413 fluorescent tubes)/8-h dark cycle; 22°C) for 4-5 weeks.

414 **Hordeum vulgare**

415 *Hordeum vulgare* (barley) was germinated in John Innes Peat & Sand Mix (85% Fine
416 Peat, 15% Grit, 2.7 kg/m^3 Agent, 4 kg/m^3 Osmocote 3 to 4 months, Wetting Maglime,
417 and 1 kg PG Mix). Barley was grown at 25 °C under a 16-h light and dark cycle in 24-
418 well trays. The first leaf was sampled at second leaf emergence at 7 days post
419 germination for *M. oryzae* detached-leaf assays. The second leaf was sampled for
420 transgene insert copy number analysis and this was performed by AttoDNA Limited
421 (Norwich, United Kingdom) using real-time PCR assaying the presence of the
422 hygromycin resistance gene.

423 **Bacterial Strains**

424 *Escherichia coli* bacteria (Stellar, SHuffle and Rosetta (DE3)) were grown on LB
425 (Lysogeny broth) plates or in liquid media with appropriate antibiotics at 37°C.
426 *Agrobacterium tumefaciens* (GV3101; C58 (rifR) Ti pMP90 (pTiC58DT-DNA) (gentR)
427 Nopaline(pSouptetR)) containing the relevant binary expression vector were grown on
428 LB (Lysogeny broth) plates or in liquid media with appropriate antibiotics at 28 ^{o}C.

429 **Yeast Strains**

430 The *Saccharomyces cerevisiae* strain Y2HGold (Takara Bio, Cat. No. 630489) was
431 used in this study. Yeast cultures were grown on plates or liquid in SD minimal media
432 SD/-Leu and SD/-Trp. Plates containing SD/–Ade/–His/–Leu/–Trp dropout supplement
433 were used for the activation of *HIS3 and ADE2* to identify positive interactions via
434 Yeast-two-hybrid. All Yeast was grown at 30 °C

435 ***Magnaporthe oryzae***

436 *Magnaporthe oryzae* isolates were grown and transformed as described[32,53]. Briefly,
437 cultures were revived from frozen stocks on filter paper at -20°C and maintained on
438 potato dextrose agar medium at 24 °C under a 16hr light cycle. The isolates BTJP 4-
439 1, Sasa2, and transgenic Sasa2 transformed with AVR-Pii^{Wb} (ZiF_VIIIc) were used in
440 plant inoculations.

441 ## Method details

442 **Transcriptome assembly and phylogenetic analysis**

443 Publicly available RNAseq data sets for Poales species were identified from NCBI SRA
444 database and *de novo* transcriptome assemblies were generated using Trinity with
445 default parameters (version 2013-11-10). The Poales species phylogenetic tree was
446 generated using the QKbusco pipeline (https://github.com/matthewmoscou/QKbusco)
447 as described in Brabham *et al.,* (2024)[53]. Briefly, open reading frames from assemblies
448 predicted using TransDecoder (v4.1.0). Benchmarking universal single-copy orthologs
449 were identified using BUSCO (v3.0.2) with default parameters and embryophyte_odb9
450 library. Genes identified with BUSCO were used to generate a multiple sequence
451 alignment using QKbusco_merge.py using parameter 'allfragmented'. Codon-based
452 multiple sequence alignment was performed with PRANK (v.170427) using default
453 parameters. Multiple sequence alignments were merged using
454 QKbusco_phylogeny.py with coverage depth of 40% at individual sites. The maximum
455 likelihood phylogenetic tree was generated using RAxML (v8.2.12) with the
456 GTRGAMMA model.
457 InterProScan (v5.27-66.0) using default parameters was used to identify NB-ARC
458 (Pfam PF00027 and PF00931) and Exo70 (Pfam PF03081) domain containing
459 proteins from *de novo* transcriptomes predicted proteins from TransDecoder. Domain

460 boundaries of integrated NLRs were manually curated based on Pfam annotation.
461 Phylogenetic analysis of Exo70 domains was carried out as described by Holden *et*
462 *al.*, (2022)[43]. Briefly, structure-guided multiple sequence alignment was performed with
463 MAFFT software (v7.481) using DASH (Database of Aligned Structural Homologs)
464 with default parameters. Structurally resolved Exo70 structures included *A. thaliana*
465 Exo70A1 (PDB 4RL5), *S. cerevisiae* (yeast) Exo70 (PDB 2B1E and 5YFP), and *Mus*
466 *musculus* (mouse) (PDB 2PFT). The maximum likelihood phylogenetic tree was
467 constructed using RAxML (v8.2.12) with the JTT amino acid substitution model,
468 gamma model of rate heterogeneity, and 1,000 bootstraps. iTOL (Interactive Tree of
469 Life) was used for phylogenetic tree visualization, and *S. cerevisiae* and *M. musculus*
470 Exo70 were used as outgroups.
471
472 **Cell death assay**

473 Four-week-old *N. benthamiana* plants were simultaneously infiltrated with
474 Agrobacteria carrying the relevant constructs *35Spro::*RGH2-FLAG, *35Spro::*RGH2^{+}-
475 FLAG, *35Spro::*RGH3-HA and *MASpro::*GFP-AVR-Pii from wheat and rice or
476 *35Spro::*GFP-HA and *MASpro::*GFP-AVR-Pii^{F65E} as controls. The Agrobacterium
477 strains were resuspended in ARM buffer (Agrobacterium resuspension medium)
478 containing 10 mM MES (pH 5.6), 10 mM MgCl2, and 150 μM acetosyringone. The
479 optical density at 600 nm (OD_{600}) was adjusted as follows: RGH2/RGH2^{+} and RGH3
480 at 0.4, effectors and controls at 0.6, and p19 at 0.1. Two leaves from each *N.*
481 *benthamiana* plant were infiltrated using a needleless syringe. Leaves were harvested
482 at 3 days post-infiltration (dpi), and UV fluorescence images were captured from the
483 abaxial side. Imaging was conducted using a Nikon D4 camera equipped with a 60-
484 mm macro lens, with ISO set at 1600 and an exposure time of approximately 10
485 seconds at F14. A Kodak Wratten No.8 filter was used, and the white balance was set
486 to 6,250 °K. Illumination was provided by Blak–Ray longwave (365 nm) B-100AP
487 spotlight lamps, which were moved around the subject during exposure to ensure even
488 illumination. The presented images are representative of three independent
489 experiments, each with a minimum of 6 leaves analysed.

490

491 **Ion leakage assays**

492 Leaves of *N. benthamiana* were infiltrated with either *35Spro::*RGH2-FLAG or
493 *35Spro::*RGH2^{+}-FLAG in combination with *MASpro::*RGH3-HA and either
494 *MASpro::*GFP-AVR-Pii or *MASpro::*GFP-AVR-Pii$^{Phe/Glu}$ from both rice and wheat blast.
495 Ion leakage assays were performed as described in Hatsugai and Katagiri (2018)[67].
496 Briefly, measurements were performed after 4, 24 and 48 hours post-harvest with a
497 compact conductivity meter (LAQUAtwin-EC-33, Horiba Scientific). Five leaf discs
498 (4mm diameter) were harvested from different leaves and immersed inside 2ml ddH_2O
499 as one biological replicate. Each measurement contains five biological replicates, and
500 all experiments were performed at least three times.

501 **Split GAL4 RUBY assay**

502 To detect protein-protein binding in *N. benthamiana* we performed the split GAL4
503 RUBY assay according to Chen *et al*., 2023.[51] Briefly, Agrobacterium containing
504 OsExo70F3, RGH2-Exo70 and RGH2^{+}-Exo70 (residues 1033-1637) fused to the
505 yeast GAL4 DNA binding domain protein under the *35S* promoter. Wheat and rice blast
506 AVR-Pii and the mutants or ZiF_IIb were fused to the herpes virus VP16 AD either
507 under the *35S* promoter or *MAS* promoter. *N. benthamiana* leaves were harvested
508 after 3dpi. To extract betalain, harvested plant leaves were completely immersed in
509 100% ethanol until all chlorophyll was removed. A diameter of 0.8 cm was taken from
510 each infiltration site and put into H_20. Extracted betalain accumulation was measured
511 in a Greiner F-bottom clear plate in a microplate reader (Clariostar, BMG Labtech) at
512 538 nm wavelength. All experiments were performed with five plants and repeated at
513 least 3 times.

514 To confirm protein expression, plant samples were harvested 3 dpi, ground in liquid
515 nitrogen and heated for 10 min at 70 °C in LDS buffer (Bio-Rad Laboratories, USA).
516 Samples were centrifugated and the supernatant was subjected to SDS-PAGE gels
517 and western blot. The membranes were probed with anti-GAL4 DNA-BD (Sigma-
518 Aldrich) for OsExo70F3, RGH2-Exo70 and RGH2^{+}-Exo70 and with the anti-VP16
519 antibody (Sigma-Aldrich, USA, V4388) antibodies for the effectors.

520

521 **Co-immunoprecipitation**

522 Transient gene expression in planta was performed by co-infiltrating 4-week-old *N.*
523 *benthamiana* plants with *A. tumefaciens* strain GV3101 carrying *35Spro::*OsExo70F3-
524 FLAG or *35Spro::*RGH2-Exo70-FLAG with rice AVR-Pii, the wheat blast variant or their
525 respective mutants. NLRs *MASpro::*FLAG-RGH2, *MASpro::*FLAG-RGH2^{+},
526 *MASpro::*HA-RGH3 and rice AVR-Pii, the wheat blast variant, or their respective
527 mutants, and ZiF_IIb under the *MAS* promoter (Figure 3D and Figure S9) were
528 infiltrated at OD_{600} 0.4 and 0.6, respectively, in ARM buffer (Agrobacterium
529 resuspension medium, 10 mM MgCl2, 10 mM 2-(N-morpholine)-ethanesulfonic acid
530 [MES], and pH 5.6) with the addition of 150 μM acetosyringone. Two leaves from each
531 *N. benthamiana* plant were infiltrated and 72 h later, samples were harvested and
532 frozen in liquid nitrogen. Total proteins were extracted from 450 mg tissue samples
533 and suspended in 2 mL GTEN buffer (25 mM Tris pH 7.5, 150 mM NaCl, 1 mM EDTA,
534 10% v/v glycerol, 2% w/v PVPP, 10 mM DTT, 1 × complete protease inhibitor tablet
535 per 50 mL (Roche), and 0.1% Tween 20). Extracts were cleared by centrifugation at
536 4000 xg at 4 °C for 30 min. Protein pull downs were performed by adding 30 μL of anti-
537 FLAG magnetic beads using M2 anti-FLAG magnetic beads (Sigma). Briefly, samples
538 were incubated in a rotary mixer for 3h at 4 °C, washed afterwards 5 times with 1 ml
539 IP buffer (25 mM Tris pH 7.5, 150 mM NaCl, 1 mM EDTA, 10% glycerol, and 0.1%
540 Tween 20) and proteins were eluted by incubating the beads at 70°C in 30 μL of LDS
541 RunBlue sample buffer for 10 mins. About 15–20 μL of the extracts were analysed by
542 SDS-PAGE followed by immunoblot using either anti-FLAG (Cohesion Biosciences, at
543 1:3000 dilution), anti-GFP (Santa Cruz Biotechnology, at 1:3000 dilution) or HA-probe
544 (Santa Cruz Biotechnology, 1:5000 dilution). Experiments were repeated at least three
545 times.

546 **Protein immunoblotting**

547 Protein samples were prepared from five tissue discs (8 mm diameter) sampled from
548 *N. benthamiana* leaves at 2 or 3 days after agroinfiltration and were homogenized in
549 100 μL of 2X LDS loading buffer (Bio-Rad). Proteins were transferred onto a PVDF
550 (polyvinylidene difluoride) membrane using Trans-Blot Turbo transfer system (Bio-
551 Rad) according to the manufacturer's protocol. Immunoblotting was performed with
552 HA-probe (Santa Cruz Biotechnology, 1:5000 dilution), anti-GFP antibody ((Santa

553 Cruz Biotechnology, at 1:3000 dilution) or anti-FLAG (Cohesion Biosciences, at 1:3000
554 dilution). Proteins were visualized using Clarity Max Western ECL Substrate (Bio Rad)
555 in the ImageQuant LAS 500 spectrophotometer (GE Healthcare). Total protein loading
556 was visualized by staining the PVDF membrane with Ponceau S solution (Sigma-
557 Aldrich, P7170).

558 **Yeast two-hybrid assay**

559 To examine the interaction between all Exo70s and effectors we used the Matchmaker
560 Gold system (Takara Bio, USA) following the manufacturer's protocol. The proteins
561 were cloned into pGBKT7 or pGADT7 vectors, respectively. Exo70 integrated domains
562 RGH2-Exo70 (residues 1033-1637), RGH2^{+}-Exo70 (residues 1033-1637), Apu28443-
563 Exo70 (residues 990-1644), Hla80948-Exo70 (residues 765-1269), Hvu23924-Exo70
564 (residues 726-1321), Jef9120-Exo70 (residues 364-887) were cloned into pGBKT7 for
565 GAL4 binding domain fusion. OsExo70F3 in pGBKT7 and ZiF effectors and mutants
566 in pGADT7 were previously generated[32]. Constructs were co-transformed into
567 chemically competent Y2HGold cells using a Frozen-EZ Yeast transformation II Kit
568 (Zymo research, USA). We selected yeast co-transformants on selective dropout (SD)
569 media lacking only Trp and Leu. Protein interactions were assessed on SD selection
570 medium lacking Trp, Leu, His and Ade containing X-α-Gal and supplemented with 0.2
571 ug/ml Aureobasidin A (Takara Bio, USA). Plates were incubated on 30 °C and
572 interaction was observed 4 days later. Each experiment was repeated a minimum of
573 three times with similar results.

574 To confirm protein expression, total yeast extracts from transformed colonies were
575 produced by heating the cells for 10 min at 70 °C in LDS buffer (Bio-Rad Laboratories,
576 USA). Samples were centrifugated and the supernatant was subjected to SDS-PAGE
577 gels and western blot. The membranes were probed with anti-GAL4 DNA-BD (Sigma)
578 for OsExo70F3, RGH2-Exo70, RGH2^{+}-Exo70, Apu28443-Exo70, Hla80948-Exo70,
579 Hvu23924-Exo70, Jef9120-Exo70 proteins in pGBKT7 and with the anti-GAL4
580 activation domain (Sigma) antibodies for effectors in pGADT7.

581 **Protein expression and purification**

582 RGH2-Exo70 and RGH2^{+}-Exo70 domains (residues 1033-1637) were 6xHis-SUMO-
583 tagged and produced in *E. coli* Rosetta™ (DE3) and AVR-Pii variants were 6xHis-
584 MBP-tagged and produced in *E. coli* SHuffle cells using established protocols[29]. All

585 tags were added at the N-terminus. In brief, cell cultures were grown in LB media at
586 37 °C for Rosetta and 30 °C for SHuffle cells for 5–7 hr and then at 16 °C overnight.
587 Cells were harvested by centrifugation (10 min, 5500x g, 4 °C) and re-suspended in
588 50 mM Tris-HCl (pH 7.5), 500 mM NaCl, 50 mM glycine, 5% (vol/vol) glycerol, and 20
589 mM imidazole supplemented with cOmplete EDTA-free Protease Inhibitor Cocktail
590 (Roche). Cells were lysed by sonication and clarified by centrifugation (50,000x g for
591 30 mins at 4 °C). Protein purification was carried out as previously described[29].

592 **Isothermal titration calorimetry**

593 ITC experiments were performed using a MicroCal PEAQ-ITC instrument (Malvern,
594 United Kingdom). For each experiment, 300µL of RGH2-Exo70 or RGH2^{+}-Exo70
595 domains at a concentration of 20 µM was loaded into the calorimetric cell, while the
596 syringe contained 200 µM of either wheat or rice blast AVR-Pii or their Phe to Glu
597 mutants. Each run consisted of a single injection of 0.5 µL followed by 18 injections of
598 2 µL each, with intervals of 120 s between injections. The stirring speed was 750 rpm.
599 Data obtained from the experiments were analysed using AFFINImeter ITC software[68].
600 Both wild type and mutant samples were subjected to triplicate runs. The experiments
601 were conducted at 25 °C in a buffer containing 20 mM HEPES (pH 7.5), 150 mM NaCl,
602 and 5% (vol/vol) glycerol. The stability of RGH2/RGH2^{+} Exo70 domains on purification
603 likely affects the accurate measurement of stoichiometry on complex formation with
604 the effectors (1:1 expected based on the structure of OsExo70F2 with AVR-Pii).

605 ***M. oryzae* inoculation and plant phenotypic assays**

606 Protocols for culturing and inoculation of *M. oryzae* were similar to those previously
607 described[46,69,70] Briefly, hyphal tips from culture plates were transferred to oatmeal
608 agar (20 g oatmeal, 10 g agar, 2.5 g sucrose, and addition of ddH2O to 500 mL) plates
609 (deep petri dish 100 × 20 mm) and incubated for 10 to 15 d at 24 °C to produce conidia.
610 Oatmeal plates were washed with 8 mL dH2O and conida collected by gentle scraping
611 with the tip of a 1.5-mL tube. The suspension was filtered through Miracloth (Merck
612 Chemicals, Ref.: 475855-1r) and collected. Spore concentration was counted via
613 hemocytometer and adjusted to 1×10^5 spores per milliliter in dH2O with 0.01% Tween
614 20 (Merck Chemicals, CAS Number: 9005-64-5).

615 For detached leaf assays, barley leaves were sampled and placed on agar in boxes
616 (2.5 g agar-agar [Fisher, CAS 9002-18-0]; 50 mL benzimidazole [1 g/1 L H2O stock

solution]; 450 mL H2O). For spot inoculations, 5 µL of conidial suspension of each isolate was placed on the leaf. For spray inoculations, the conidial suspension was sprayed onto the leaves in each box using a small atomiser spray bottle with approximately 3 - 4 sprays used until droplets were observed on the leaf surface. Boxes were placed in a Sanyo cabinet and maintained at 25 °C. Continuous light was used in the first 24 hrs and then, after excess water was removed from droplets using sterile Miracloth, boxes were maintained in a 16/8 hr light and dark cycle. Phenotypes were recorded at 7 dpi using a macroscopic phenotype scale[46] (0 = complete resistance; 1 = small brown resistant spots; 2 = susceptible larger eyespot lesions; 3 = larger spreading lesions; and 4 = hypersusceptibility) and by measuring lesion size (Fiji).

Statistical analyses

Graphs and statistical analysis (the Student's *t* test, Tukey's ANOVA and Two-Way ANOVA) were performed using GraphPad Prism version 10.2.2 and R-Studio version 2024.04.2+764. Details of plots and statistical tests used are given in the appropriate figure legends.

Resource availability

Lead contact

Further information and requests for resources and reagents should be directed to the lead contact Mark Banfield (mark.banfield@jic.ac.uk).

Materials availability

There are no restrictions on the availability of materials. All materials are available from the lead contact. Any additional information required to re-analyze the data reported in this paper is available from the lead contact.

Data and code availability

Data including FASTA, Phylip, and Nexus files used for preparing Figure 1 are available on Figshare (www.doi.org/10.6084/m9.figshare.28057085). All other study data are included in the article and/or Supplementary Information

Acknowledgments

The authors thank the Biotechnology and Biological Sciences Research Council (UKRI-BBSRC, UK, grants BB/V015508/1, BB/P012574, BBS/E/J/000PR9795, BBS/E/J/000PR9796 and BB/X010996/1), the BBSRC Norwich Research Park Biosciences Doctoral Training Partnership (grant BB/T008717/1), the John Innes Foundation, the Gatsby Charitable Foundation, the United States Department of Agriculture-Agricultural Research Service (CRIS #5062-21220-025-000D) and the European Union Framework Programme for Research and Innovation Horizon 2020 (2014–2020) under the Marie Curie Skłodowska Grant Agreement Nr. 847548 for funding. The authors thank all members of the Banfield Laboratory for discussions, in particular Clemence Rodney for careful reading of the manuscript. The authors also thank Abbas Maqbool (JIC Biophysical Analysis), Carlo Martins and Gerhard Saalbach (JIC Proteomics), Julia Mundy (JIC Structural Biology), Phil Robinson (Scientific Photographer), Matt Smoker and Jodie Taylor (TSL Tissue Culture and Transformation), Mark Youles and Liam Egan (TSL SynBio) for their expert help and advice in this work.

Author Contributions:

I.S., H.J.B., M.J.M., J.C.D.C. and M.J.B. designed the experiments; I.S., H.J.B., J.W.B., A.H.C.L., I.H, M.J.M. and J.C.D.C. performed the experiments; I.S., H.J.B., J.W.B., A.H.C.L., I.H., M.J.M., J.C.D.C. and M.J.B. wrote and reviewed the manuscript.

Declaration of Interests

The authors declare no competing interests.

References

(1) Wilson, R. A.; Talbot, N. J. Under Pressure: Investigating the Biology of Plant Infection by Magnaporthe Oryzae. *Nat. Rev. Microbiol.* **2009**, *7* (3), 185–195. https://doi.org/10.1038/nrmicro2032.

(2) Latorre, S. M.; Were, V. M.; Foster, A. J.; Langner, T.; Malmgren, A.; Harant, A.; Asuke, S.; Reyes-Avila, S.; Gupta, D. R.; Jensen, C.; Ma, W.; Mahmud, N. U.; Mehebub, M. S.; Mulenga, R. M.; Muzahid, A. N. M.; Paul, S. K.; Rabby, S. M. F.; Rahat, A. A. M.; Ryder, L.; Shrestha, R.-K.; Sichilima, S.; Soanes, D. M.; Singh, P. K.; Bentley, A. R.; Saunders, D. G. O.; Tosa, Y.; Croll, D.; Lamour, K. H.; Islam, T.; Tembo, B.; Win, J.; Talbot, N. J.; Burbano, H. A.; Kamoun, S. Genomic Surveillance Uncovers a Pandemic Clonal Lineage of the Wheat Blast Fungus. *PLOS Biol.* **2023**, *21* (4), e3002052. https://doi.org/10.1371/journal.pbio.3002052.

(3) Maciel, J. L. N. Magnaporthe Oryzae, the Blast Pathogen: Current Status and Options for Its Control. *CABI Rev.* **2012**, *2011*, 1–8. https://doi.org/10.1079/PAVSNNR20116050.

(4) Igarashi, S. Pyricularia Em Trigo. 1. Ocorrencia de Pyricularia Sp Noestado Do Parana. *Fitopatol.Bras* **1986**, *11*, 351–352.

(5) Singh, P. K.; Gahtyari, N. C.; Roy, C.; Roy, K. K.; He, X.; Tembo, B.; Xu, K.; Juliana, P.; Sonder, K.; Kabir, M. R.; Chawade, A. Wheat Blast: A Disease Spreading by Intercontinental Jumps and Its Management Strategies. *Front. Plant Sci.* **2021**, *12*. https://doi.org/10.3389/fpls.2021.710707.

(6) Bentham, A. R.; De la Concepcion, J. C.; Benjumea, J. V.; Kourelis, J.; Jones, S.; Mendel, M.; Stubbs, J.; Stevenson, C. E. M.; Maidment, J. H. R.; Youles, M.; Zdrzałek, R.; Kamoun, S.; Banfield, M. J. Allelic Compatibility in Plant Immune Receptors Facilitates Engineering of New Effector Recognition Specificities. *Plant Cell* **2023**, *35* (10), 3809–3827. https://doi.org/10.1093/plcell/koad204.

(7) Kourelis, J.; Marchal, C.; Posbeyikian, A.; Harant, A.; Kamoun, S. NLR Immune Receptor–Nanobody Fusions Confer Plant Disease Resistance. *Science* **2023**, *379* (6635), 934–939. https://doi.org/10.1126/science.abn4116.

(8) Zdrzałek, R.; Stone, C.; De la Concepcion, J. C.; Banfield, M. J.; Bentham, A. R. Pathways to Engineering Plant Intracellular NLR Immune Receptors. *Curr. Opin. Plant Biol.* **2023**, *74*, 102380. https://doi.org/10.1016/j.pbi.2023.102380.

(9) Cadiou, L.; Brunisholz, F.; Cesari, S.; Kroj, T. Molecular Engineering of Plant Immune Receptors for Tailored Crop Disease Resistance. *Curr. Opin. Plant Biol.* **2023**, *74*, 102381. https://doi.org/10.1016/j.pbi.2023.102381.

(10) Jones, J. D. G.; Vance, R. E.; Dangl, J. L. Intracellular Innate Immune Surveillance Devices in Plants and Animals. *Science* **2016**, *354* (6316), aaf6395. https://doi.org/10.1126/science.aaf6395.

(11) Jubic, L. M.; Saile, S.; Furzer, O. J.; El Kasmi, F.; Dangl, J. L. Help Wanted: Helper NLRs and Plant Immune Responses. *Curr. Opin. Plant Biol.* **2019**, *50*, 82–94. https://doi.org/10.1016/j.pbi.2019.03.013.

(12) Adachi, H.; Derevnina, L.; Kamoun, S. NLR Singletons, Pairs, and Networks: Evolution, Assembly, and Regulation of the Intracellular Immunoreceptor Circuitry of Plants. *Curr. Opin. Plant Biol.* **2019**, *50*, 121–131. https://doi.org/10.1016/j.pbi.2019.04.007.

(13) Ashikawa, I.; Hayashi, N.; Yamane, H.; Kanamori, H.; Wu, J.; Matsumoto, T.; Ono, K.; Yano, M. Two Adjacent Nucleotide-Binding Site–Leucine-Rich Repeat Class Genes Are Required to Confer Pikm-Specific Rice Blast Resistance. *Genetics* **2008**, *180* (4), 2267–2276. https://doi.org/10.1534/genetics.108.095034.

(14) Maqbool, A.; Saitoh, H.; Franceschetti, M.; Stevenson, C.; Uemura, A.; Kanzaki, H.; Kamoun, S.; Terauchi, R.; Banfield, M. Structural Basis of Pathogen Recognition by an Integrated HMA Domain in a Plant NLR Immune Receptor. *eLife* **2015**, *4*, e08709. https://doi.org/10.7554/eLife.08709.

(15) Césari, S.; Thilliez, G.; Ribot, C.; Chalvon, V.; Michel, C.; Jauneau, A.; Rivas, S.; Alaux, L.; Kanzaki, H.; Okuyama, Y.; Morel, J.-B.; Fournier, E.; Tharreau, D.; Terauchi, R.; Kroj, T. The Rice Resistance Protein Pair RGA4/RGA5 Recognizes the Magnaporthe Oryzae Effectors AVR-Pia and AVR1-CO39 by Direct Binding. *Plant Cell* **2013**, *25* (4), 1463–1481. https://doi.org/10.1105/tpc.112.107201.

(16) Césari, S.; Kanzaki, H.; Fujiwara, T.; Bernoux, M.; Chalvon, V.; Kawano, Y.; Shimamoto, K.; Dodds, P.; Terauchi, R.; Kroj, T. The NB-LRR Proteins RGA4 and RGA5 Interact Functionally and Physically to Confer Disease Resistance. *EMBO J.* **2014**, *33* (17), 1941–1959. https://doi.org/10.15252/embj.201487923.

(17) Zhang, X.; Liu, Y.; Yuan, G.; Wang, D.; Zhu, T.; Wu, X.; Ma, M.; Guo, L.; Guo, H.; Bhadauria, V.; Liu, J.; Peng, Y.-L. The Effector Recognition by Synthetic Sensor NLR Receptors Requires the Concerted Action of Multiple Interfaces within and Outside the Integrated Domain. bioRxiv August 18, 2022, p 2022.08.17.504349. https://doi.org/10.1101/2022.08.17.504349.

(18) De la Concepcion, J. C.; Franceschetti, M.; Maqbool, A.; Saitoh, H.; Terauchi, R.; Kamoun, S.; Banfield, M. J. Polymorphic Residues in Rice NLRs Expand Binding and Response to Effectors of the Blast Pathogen. *Nat. Plants* **2018**, *4* (8), 576–585. https://doi.org/10.1038/s41477-018-0194-x.

(19) De la Concepcion, J. C.; Franceschetti, M.; MacLean, D.; Terauchi, R.; Kamoun, S.; Banfield, M. J. Protein Engineering Expands the Effector Recognition Profile of a Rice NLR Immune Receptor. *eLife* **2019**, *8*, e47713. https://doi.org/10.7554/eLife.47713.

(20) Maidment, J. H.; Shimizu, M.; Bentham, A. R.; Vera, S.; Franceschetti, M.; Longya, A.; Stevenson, C. E.; De la Concepcion, J. C.; Białas, A.; Kamoun, S.; Terauchi, R.; Banfield, M. J. Effector Target-Guided Engineering of an Integrated Domain Expands the Disease Resistance Profile of a Rice NLR Immune Receptor. *eLife* **2023**, *12*, e81123. https://doi.org/10.7554/eLife.81123.

(21) Kanzaki, H.; Yoshida, K.; Saitoh, H.; Fujisaki, K.; Hirabuchi, A.; Alaux, L.; Fournier, E.; Tharreau, D.; Terauchi, R. Arms Race Co-Evolution of Magnaporthe Oryzae AVR-Pik and Rice Pik Genes Driven by Their Physical Interactions. *Plant J.* **2012**, *72* (6), 894–907. https://doi.org/10.1111/j.1365-313X.2012.05110.x.

(22) De la Concepcion, J. C.; Vega Benjumea, J.; Bialas, A.; Terauchi, R.; Kamoun, S.; Banfield, M. J. Functional Diversification Gave Rise to Allelic Specialization in a Rice NLR Immune Receptor Pair. *eLife* **2021**, *10*, e71662. https://doi.org/10.7554/eLife.71662.

(23) Maidment, J. H. R.; Franceschetti, M.; Maqbool, A.; Saitoh, H.; Jantasuriyarat, C.; Kamoun, S.; Terauchi, R.; Banfield, M. J. Multiple Variants of the Fungal Effector AVR-Pik Bind the HMA Domain of the Rice Protein OsHIPP19, Providing a Foundation to Engineer Plant Defense. *J. Biol. Chem.* **2021**, *296*. https://doi.org/10.1016/j.jbc.2021.100371.

(24) Zdrzałek, R.; Xi, Y.; Langner, T.; Bentham, A. R.; Petit-Houdenot, Y.; De la Concepcion, J. C.; Harant, A.; Shimizu, M.; Were, V.; Talbot, N. J.; Terauchi, R.; Kamoun, S.; Banfield, M. J. Bioengineering a Plant NLR Immune Receptor with a Robust Binding Interface toward a Conserved Fungal Pathogen Effector. *Proc. Natl. Acad. Sci.* **2024**, *121* (28), e2402872121. https://doi.org/10.1073/pnas.2402872121.

(25) Guo, L.; Cesari, S.; de Guillen, K.; Chalvon, V.; Mammri, L.; Ma, M.; Meusnier, I.; Bonnot, F.; Padilla, A.; Peng, Y.-L.; Liu, J.; Kroj, T. Specific Recognition of Two MAX Effectors by Integrated HMA Domains in Plant Immune Receptors Involves Distinct Binding Surfaces. *Proc. Natl. Acad. Sci.* **2018**, *115* (45), 11637–11642. https://doi.org/10.1073/pnas.1810705115.

(26) Okuyama, Y.; Kanzaki, H.; Abe, A.; Yoshida, K.; Tamiru, M.; Saitoh, H.; Fujibe, T.; Matsumura, H.; Shenton, M.; Galam, D. C.; Undan, J.; Ito, A.; Sone, T.; Terauchi, R. A Multifaceted Genomics Approach Allows the Isolation of the Rice Pia-Blast Resistance Gene Consisting of Two Adjacent NBS-LRR Protein Genes. *Plant J.* **2011**, *66* (3), 467–479. https://doi.org/10.1111/j.1365-313X.2011.04502.x.

(27) Ortiz, D.; de Guillen, K.; Cesari, S.; Chalvon, V.; Gracy, J.; Padilla, A.; Kroj, T. Recognition of the Magnaporthe Oryzae Effector AVR-Pia by the Decoy Domain of the Rice NLR Immune Receptor RGA5. *Plant Cell* **2017**, *29* (1), 156–168. https://doi.org/10.1105/tpc.16.00435.

(28) Liu, Y.; Zhang, X.; Yuan, G.; Wang, D.; Zheng, Y.; Ma, M.; Guo, L.; Bhadauria, V.; Peng, Y.-L.; Liu, J. A Designer Rice NLR Immune Receptor Confers Resistance to the Rice Blast Fungus Carrying Noncorresponding Avirulence Effectors. *Proc. Natl. Acad. Sci.* **2021**, *118* (44), e2110751118. https://doi.org/10.1073/pnas.2110751118.

(29) De la Concepcion, J. C.; Fujisaki, K.; Bentham, A. R.; Cruz Mireles, N.; Sanchez de Medina Hernandez, V.; Shimizu, M.; Lawson, D. M.; Kamoun, S.; Terauchi, R.; Banfield, M. J. A Blast Fungus Zinc-Finger Fold Effector Binds to a Hydrophobic Pocket in Host Exo70 Proteins to Modulate Immune Recognition in Rice. *Proc. Natl. Acad. Sci.* **2022**, *119* (43), e2210559119. https://doi.org/10.1073/pnas.2210559119.

(30) Fujisaki, K.; Abe, Y.; Ito, A.; Saitoh, H.; Yoshida, K.; Kanzaki, H.; Kanzaki, E.; Utsushi, H.; Yamashita, T.; Kamoun, S.; Terauchi, R. Rice Exo70 Interacts with a Fungal Effector, AVR-Pii, and Is Required for AVR-Pii-Triggered Immunity. *Plant J.* **2015**, *83* (5), 875–887. https://doi.org/10.1111/tpj.12934.

(31) Fujisaki, K.; Abe, Y.; Sugihara, Y.; Nemoto, K.; Ito, K.; Kanzaki, E.; Ishikawa, K.; Iwai, M.; Utsushi, H.; Saitoh, H.; Takagi, H.; Takeda, T.; Abe, A.; Zheng, S.; Bialas, A.; Banfield, M. J.; Kamoun, S.; Terauchi, R. Binding of a Pathogen Effector to Rice Exo70 Proteins Tethered to the NOI/RIN4 Integrated Domain of the NLR Receptor Pii2 Confers Immunity against Fungi. bioRxiv August 27, 2024, p 239400. https://doi.org/10.1101/239400.

(32) De la Concepcion, J. C.; Langner, T.; Fujisaki, K.; Yan, X.; Were, V.; Lam, A. H. C.; Saado, I.; Brabham, H. J.; Win, J.; Yoshida, K.; Talbot, N. J.; Terauchi, R.; Kamoun, S.; Banfield, M. J. Zinc-Finger (ZiF) Fold Secreted Effectors Form a Functionally Diverse Family across Lineages of the Blast Fungus Magnaporthe Oryzae. *PLOS Pathog.* **2024**, *20* (6), e1012277. https://doi.org/10.1371/journal.ppat.1012277.

(33) Saeed, B.; Brillada, C.; Trujillo, M. Dissecting the Plant Exocyst. *Curr. Opin. Plant Biol.* **2019**, *52*, 69–76. https://doi.org/10.1016/j.pbi.2019.08.004.

(34) Mei, K.; Guo, W. The Exocyst Complex. *Curr. Biol.* **2018**, *28* (17), R922–R925. https://doi.org/10.1016/j.cub.2018.06.042.

(35) Cvrčková, F.; Grunt, M.; Bezvoda, R.; Hála, M.; Kulich, I.; Rawat, A.; Zárský, V. Evolution of the Land Plant Exocyst Complexes. *Front. Plant Sci.* **2012**, *3*, 159. https://doi.org/10.3389/fpls.2012.00159.

(36) Žárský, V.; Sekereš, J.; Kubátová, Z.; Pečenková, T.; Cvrčková, F. Three Subfamilies of Exocyst EXO70 Family Subunits in Land Plants: Early Divergence and Ongoing Functional Specialization. *J. Exp. Bot.* **2020**, *71* (1), 49–62. https://doi.org/10.1093/jxb/erz423.

(37) Žárský, V.; Kulich, I.; Fendrych, M.; Pečenková, T. Exocyst Complexes Multiple Functions in Plant Cells Secretory Pathways. *Curr. Opin. Plant Biol.* **2013**, *16* (6), 726–733. https://doi.org/10.1016/j.pbi.2013.10.013.

(38) De la Concepcion, J. C.; Duverge, H.; Kim, Y.; Julian, J.; Xu, H. D.; Ikene, S. A.; Bianchi, A.; Grujic, N.; Papareddy, R. K.; Grishkovskaya, I.; Haselbach, D.; Murray, D. H.; Clavel, M.; Irwin, N. A. T.; Dagdas, Y. Electrostatic Changes Enabled the Diversification of an Exocyst Subunit via Protein Complex Escape. bioRxiv August 26, 2024, p 2024.08.26.609756. https://doi.org/10.1101/2024.08.26.609756.

(39) Stegmann, M.; Anderson, R. G.; Westphal, L.; Rosahl, S.; McDowell, J. M.; Trujillo, M. The Exocyst Subunit Exo70B1 Is Involved in the Immune Response of Arabidopsis Thaliana to Different Pathogens and Cell Death. *Plant Signal. Behav.* **2013**, *8* (12), e27421. https://doi.org/10.4161/psb.27421.

(40) Pecenková, T.; Hála, M.; Kulich, I.; Kocourková, D.; Drdová, E.; Fendrych, M.; Toupalová, H.; Zársky, V. The Role for the Exocyst Complex Subunits Exo70B2 and Exo70H1 in the Plant-Pathogen Interaction. *J. Exp. Bot.* **2011**, *62* (6), 2107–2116. https://doi.org/10.1093/jxb/erq402.

(41) Guo, J.; Xu, C.; Wu, D.; Zhao, Y.; Qiu, Y.; Wang, X.; Ouyang, Y.; Cai, B.; Liu, X.; Jing, S.; Shangguan, X.; Wang, H.; Ma, Y.; Hu, L.; Wu, Y.; Shi, S.; Wang, W.; Zhu, L.; Xu, X.; Chen, R.; Feng, Y.; Du, B.; He, G. Bph6 Encodes an Exocyst-Localized Protein and Confers Broad Resistance to Planthoppers in Rice. *Nat. Genet.* **2018**, *50* (2), 297–306. https://doi.org/10.1038/s41588-018-0039-6.

(42) Du, Y.; Overdijk, E. J. R.; Berg, J. A.; Govers, F.; Bouwmeester, K. Solanaceous Exocyst Subunits Are Involved in Immunity to Diverse Plant Pathogens. *J. Exp. Bot.* **2018**, *69* (3), 655–666. https://doi.org/10.1093/jxb/erx442.

(43) Holden, S.; Bergum, M.; Green, P.; Bettgenhaeuser, J.; Hernández-Pinzón, I.; Thind, A.; Clare, S.; Russell, J. M.; Hubbard, A.; Taylor, J.; Smoker, M.; Gardiner, M.; Civolani, L.; Cosenza, F.; Rosignoli, S.; Strugala, R.; Molnár, I.; Šimková, H.; Doležel, J.; Schaffrath, U.; Barrett, M.; Salvi, S.; Moscou, M. J. A Lineage-Specific Exo70 Is Required for Receptor Kinase–Mediated Immunity in Barley. *Sci. Adv.* **2022**, *8* (27), eabn7258. https://doi.org/10.1126/sciadv.abn7258.

(44) De la Concepcion, J. C. The Exocyst Complex Is an Evolutionary Battleground in Plant-Microbe Interactions. *Curr. Opin. Plant Biol.* **2023**, *76*, 102482. https://doi.org/10.1016/j.pbi.2023.102482.

(45) Césari, S.; Bernoux, M.; Moncuquet, P.; Kroj, T.; Dodds, P. N. A Novel Conserved Mechanism for Plant NLR Protein Pairs: The 'Integrated Decoy' Hypothesis. *Front. Plant Sci.* **2014**, *5*. https://doi.org/10.3389/fpls.2014.00606.

(46) Brabham, H. J.; Gómez De La Cruz, D.; Were, V.; Shimizu, M.; Saitoh, H.; Hernández-Pinzón, I.; Green, P.; Lorang, J.; Fujisaki, K.; Sato, K.; Molnár, I.; Šimková, H.; Doležel, J.; Russell, J.; Taylor, J.; Smoker, M.; Gupta, Y. K.; Wolpert, T.; Talbot, N. J.; Terauchi, R.; Moscou, M. J. Barley MLA3 Recognizes the Host-Specificity Effector Pwl2 from Magnaporthe Oryzae. *Plant Cell* **2024**, *36* (2), 447–470. https://doi.org/10.1093/plcell/koad266.

(47) Brabham, H. J.; Hernández-Pinzón, I.; Holden, S.; Lorang, J.; Moscou, M. J. An Ancient Integration in a Plant NLR Is Maintained as a Trans-Species Polymorphism. bioRxiv December 25, 2017, p 239541. https://doi.org/10.1101/239541.

(48) Kroj, T.; Chanclud, E.; Michel-Romiti, C.; Grand, X.; Morel, J.-B. Integration of Decoy Domains Derived from Protein Targets of Pathogen Effectors into Plant Immune Receptors Is Widespread. *New Phytol.* **2016**, *210* (2), 618–626. https://doi.org/10.1111/nph.13869.

(49) Sarris, P. F.; Cevik, V.; Dagdas, G.; Jones, J. D. G.; Krasileva, K. V. Comparative Analysis of Plant Immune Receptor Architectures Uncovers Host Proteins Likely Targeted by Pathogens. *BMC Biol.* **2016**, *14* (1), 8. https://doi.org/10.1186/s12915-016-0228-7.

(50) Abramson, J.; Adler, J.; Dunger, J.; Evans, R.; Green, T.; Pritzel, A.; Ronneberger, O.; Willmore, L.; Ballard, A. J.; Bambrick, J.; Bodenstein, S. W.; Evans, D. A.; Hung, C.-C.; O'Neill, M.; Reiman, D.; Tunyasuvunakool, K.; Wu, Z.; Žemgulytė, A.; Arvaniti, E.; Beattie, C.; Bertolli, O.; Bridgland, A.; Cherepanov, A.; Congreve, M.; Cowen-Rivers, A. I.; Cowie, A.; Figurnov, M.; Fuchs, F. B.; Gladman, H.; Jain, R.; Khan, Y. A.; Low, C. M. R.; Perlin, K.; Potapenko, A.; Savy, P.; Singh, S.; Stecula, A.; Thillaisundaram, A.; Tong, C.; Yakneen, S.; Zhong, E. D.; Zielinski, M.; Žídek, A.; Bapst, V.; Kohli, P.; Jaderberg, M.; Hassabis, D.; Jumper, J. M. Accurate Structure Prediction of Biomolecular Interactions with AlphaFold 3. *Nature* **2024**, *630* (8016), 493–500. https://doi.org/10.1038/s41586-024-07487-w.

(51) Chen, J.; Luo, M.; Hands, P.; Rolland, V.; Zhang, J.; Li, Z.; Outram, M.; Dodds, P.; Ayliffe, M. A Split GAL4 RUBY Assay for Visual in Planta Detection of Protein–Protein Interactions. *Plant J.* **2023**, *114* (6), 1209–1226. https://doi.org/10.1111/tpj.16234.

(52) Islam, M. T.; Gupta, D. R.; Hossain, A.; Roy, K. K.; He, X.; Kabir, M. R.; Singh, P. K.; Khan, Md. A. R.; Rahman, M.; Wang, G.-L. Wheat Blast: A New Threat to Food Security. *Phytopathol. Res.* **2020**, *2* (1), 28. https://doi.org/10.1186/s42483-020-00067-6.

(53) Brabham, H. J.; Hernández-Pinzón, I.; Yanagihara, C.; Ishikawa, N.; Komori, T.; Matny, O. N.; Hubbard, A.; Witek, K.; Feist, A.; Numazawa, H.; Green, P.; Dreiseitl, A.; Takemori, N.; Komari, T.; Freedman, R. P.; Steffenson, B.; Esse, H. P. van; Moscou, M. J. Discovery of Functional NLRs Using Expression Level, High-Throughput Transformation, and Large-Scale Phenotyping. bioRxiv June 28, 2024, p 2024.06.25.599845. https://doi.org/10.1101/2024.06.25.599845.

(54) Callaway, E. Devastating Wheat Fungus Appears in Asia for First Time. *Nature* **2016**, *532* (7600), 421–422. https://doi.org/10.1038/532421a.

(55) Islam, M. T.; Croll, D.; Gladieux, P.; Soanes, D. M.; Persoons, A.; Bhattacharjee, P.; Hossain, Md. S.; Gupta, D. R.; Rahman, Md. M.; Mahboob, M. G.; Cook, N.; Salam, M. U.; Surovy, M. Z.; Sancho, V. B.; Maciel, J. L. N.; NhaniJúnior, A.; Castroagudín, V. L.; Reges, J. T. de A.; Ceresini, P. C.; Ravel, S.; Kellner, R.; Fournier, E.; Tharreau, D.; Lebrun, M.-H.; McDonald, B. A.; Stitt, T.; Swan, D.; Talbot, N. J.; Saunders, D. G. O.; Win, J.; Kamoun, S. Emergence of Wheat Blast in Bangladesh Was Caused by a South American Lineage of Magnaporthe Oryzae. *BMC Biol.* **2016**, *14* (1), 84. https://doi.org/10.1186/s12915-016-0309-7.

(56) Tembo, B.; Mulenga, R. M.; Sichilima, S.; M'siska, K. K.; Mwale, M.; Chikoti, P. C.; Singh, P. K.; He, X.; Pedley, K. F.; Peterson, G. L.; Singh, R. P.; Braun, H. J. Detection and Characterization of Fungus (Magnaporthe Oryzae Pathotype Triticum) Causing Wheat Blast Disease on Rain-Fed Grown Wheat (Triticum Aestivum L.) in Zambia. *PLOS ONE* **2020**, *15* (9), e0238724. https://doi.org/10.1371/journal.pone.0238724.

(57) Bohra, A.; Kilian, B.; Sivasankar, S.; Caccamo, M.; Mba, C.; McCouch, S. R.; Varshney, R. K. Reap the Crop Wild Relatives for Breeding Future Crops. *Trends Biotechnol.* **2022**, *40* (4), 412–431. https://doi.org/10.1016/j.tibtech.2021.08.009.

(58) Kim, S. H.; Qi, D.; Ashfield, T.; Helm, M.; Innes, R. W. Using Decoys to Expand the Recognition Specificity of a Plant Disease Resistance Protein. *Science* **2016**, *351* (6274), 684–687. https://doi.org/10.1126/science.aad3436.

(59) Le Roux, C.; Huet, G.; Jauneau, A.; Camborde, L.; Trémousaygue, D.; Kraut, A.; Zhou, B.; Levaillant, M.; Adachi, H.; Yoshioka, H.; Raffaele, S.; Berthomé, R.; Couté, Y.; Parker, J. E.; Deslandes, L. A Receptor Pair with an Integrated Decoy Converts Pathogen Disabling of Transcription Factors to Immunity. *Cell* **2015**, *161* (5), 1074–1088. https://doi.org/10.1016/j.cell.2015.04.025.

(60) Sarris, P. F.; Duxbury, Z.; Huh, S. U.; Ma, Y.; Segonzac, C.; Sklenar, J.; Derbyshire, P.; Cevik, V.; Rallapalli, G.; Saucet, S. B.; Wirthmueller, L.; Menke, F. L. H.; Sohn, K. H.; Jones, J. D. G. A Plant Immune Receptor Detects Pathogen Effectors That Target WRKY Transcription Factors. *Cell* **2015**, *161* (5), 1089–1100. https://doi.org/10.1016/j.cell.2015.04.024.

(61) Seong, K.; Krasileva, K. V. Prediction of Effector Protein Structures from Fungal Phytopathogens Enables Evolutionary Analyses. *Nat. Microbiol.* **2023**, *8* (1), 174–187. https://doi.org/10.1038/s41564-022-01287-6.

(62) Derbyshire, M. C.; Raffaele, S. Surface Frustration Re-Patterning Underlies the Structural Landscape and Evolvability of Fungal Orphan Candidate Effectors. *Nat. Commun.* **2023**, *14* (1), 5244. https://doi.org/10.1038/s41467-023-40949-9.

(63) Guillen, K. de; Ortiz-Vallejo, D.; Gracy, J.; Fournier, E.; Kroj, T.; Padilla, A. Structure Analysis Uncovers a Highly Diverse but Structurally Conserved Effector Family in Phytopathogenic Fungi. *PLOS Pathog.* **2015**, *11* (10), e1005228. https://doi.org/10.1371/journal.ppat.1005228.

(64) Seong, K.; Wei, W.; Vega, B.; Dee, A.; Ramirez-Bernardino, G.; Kumar, R.; Parra, L.; Krasileva, K. Engineering the Plant Intracellular Immune Receptor Sr50 to Restore Recognition of the AvrSr50 Escape Mutant. bioRxiv August 9, 2024, p 2024.08.07.607039. https://doi.org/10.1101/2024.08.07.607039.

(65) Cesari, S.; Xi, Y.; Declerck, N.; Chalvon, V.; Mammri, L.; Pugnière, M.; Henriquet, C.; de Guillen, K.; Chochois, V.; Padilla, A.; Kroj, T. New Recognition Specificity in a Plant Immune Receptor by Molecular Engineering of Its Integrated Domain. *Nat. Commun.* **2022**, *13* (1), 1524. https://doi.org/10.1038/s41467-022-29196-6.

(66) Lampropoulos, A.; Sutikovic, Z.; Wenzl, C.; Maegele, I.; Lohmann, J. U.; Forner, J. GreenGate - A Novel, Versatile, and Efficient Cloning System for Plant Transgenesis. *PLOS ONE* **2013**, *8* (12), e83043. https://doi.org/10.1371/journal.pone.0083043.

(67) Hatsugai, N.; Katagiri, F. Quantification of Plant Cell Death by Electrolyte Leakage Assay. *Bio-Protoc.* **2018**, *8* (5), e2758. https://doi.org/10.21769/BioProtoc.2758.

(68) Piñeiro, Á.; Muñoz, E.; Sabín, J.; Costas, M.; Bastos, M.; Velázquez-Campoy, A.; Garrido, P. F.; Dumas, P.; Ennifar, E.; García-Río, L.; Rial, J.; Pérez, D.; Fraga, P.; Rodríguez, A.; Cotelo, C. AFFINImeter: A Software to Analyze Molecular Recognition Processes from Experimental Data. *Anal. Biochem.* **2019**, *577*, 117–134. https://doi.org/10.1016/j.ab.2019.02.031.

(69) Parker, D.; Beckmann, M.; Enot, D. P.; Overy, D. P.; Rios, Z. C.; Gilbert, M.; Talbot, N.; Draper, J. Rice Blast Infection of Brachypodium Distachyon as a Model System to Study Dynamic Host/Pathogen Interactions. *Nat. Protoc.* **2008**, *3* (3), 435–445. https://doi.org/10.1038/nprot.2007.499.

(70) Jia, Y.; Valent, B.; Lee, F. N. Determination of Host Responses to Magnaporthe Grisea on Detached Rice Leaves Using a Spot Inoculation Method. *Plant Dis.* **2003**, *87* (2), 129–133. https://doi.org/10.1094/PDIS.2003.87.2.129.

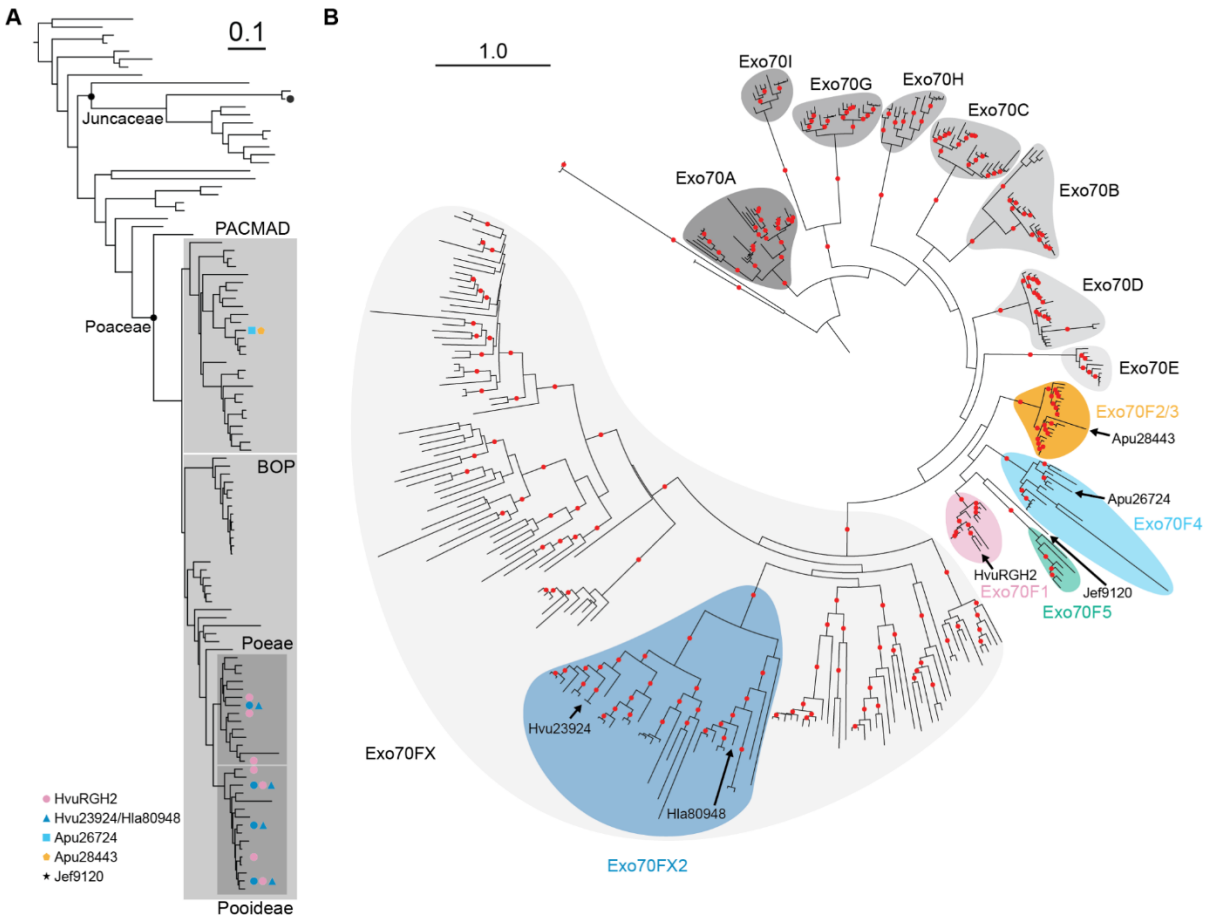

Figure 1: NLRs with integrated Exo70 domains in the Poales are derived from the Exo70F and Exo70FX clades.

A. Maximum likelihood phylogenetic tree for Poales species based on 1,019 Benchmarking Universal Single-Copy Ortholog (BUSCO) genes from 110 species spanning 1,471,281 variable sites. Outgroup species include oilpalm (*Elaeis guineensis*) and banana (*Musa acuminata*). Legend indicates the presence of integrated Exo70 domains using coloured coded shapes. Important families, clades, and subfamilies in the Poales carrying integrated Exo70 domains are indicated in shaded boxes. Scale indicates substitutions per site.

B. Maximum likelihood phylogenetic tree of grass Exo70 proteins showing that integrated Exo70 domains are derived from the Exo70F and Exo70FX clades. Grass species include barley (*Hordeum vulgare*), wheat (*Triticum aestivum*), purple false brome (*Brachypodium distachyon*), rice (*Oryza sativa*), *Oropetium thomaeum*, maize (*Zea mays*), foxtail millet (*Setaria italica*), and sorghum (*Sorghum bicolor*). Exemplar integrated Exo70 domains include *H. vulgare* RGH2 (Exo70F1) and Hvu23934

963 (Exo70FX2), *Arundinella pubescens* Apu26724 (Exo70F4) and Apu28443 (Exo70F2),
964 *Holcus lanatus* Hla80948 (Exo70FX2), and *Juncus effusus* Jef9120 (unclassified
965 Exo70F). Outgroup Exo70s include *Saccharomyces cerevisiae* (yeast) and *Mus*
966 *musculus* (mouse). Scale indicates substitutions per site.

967

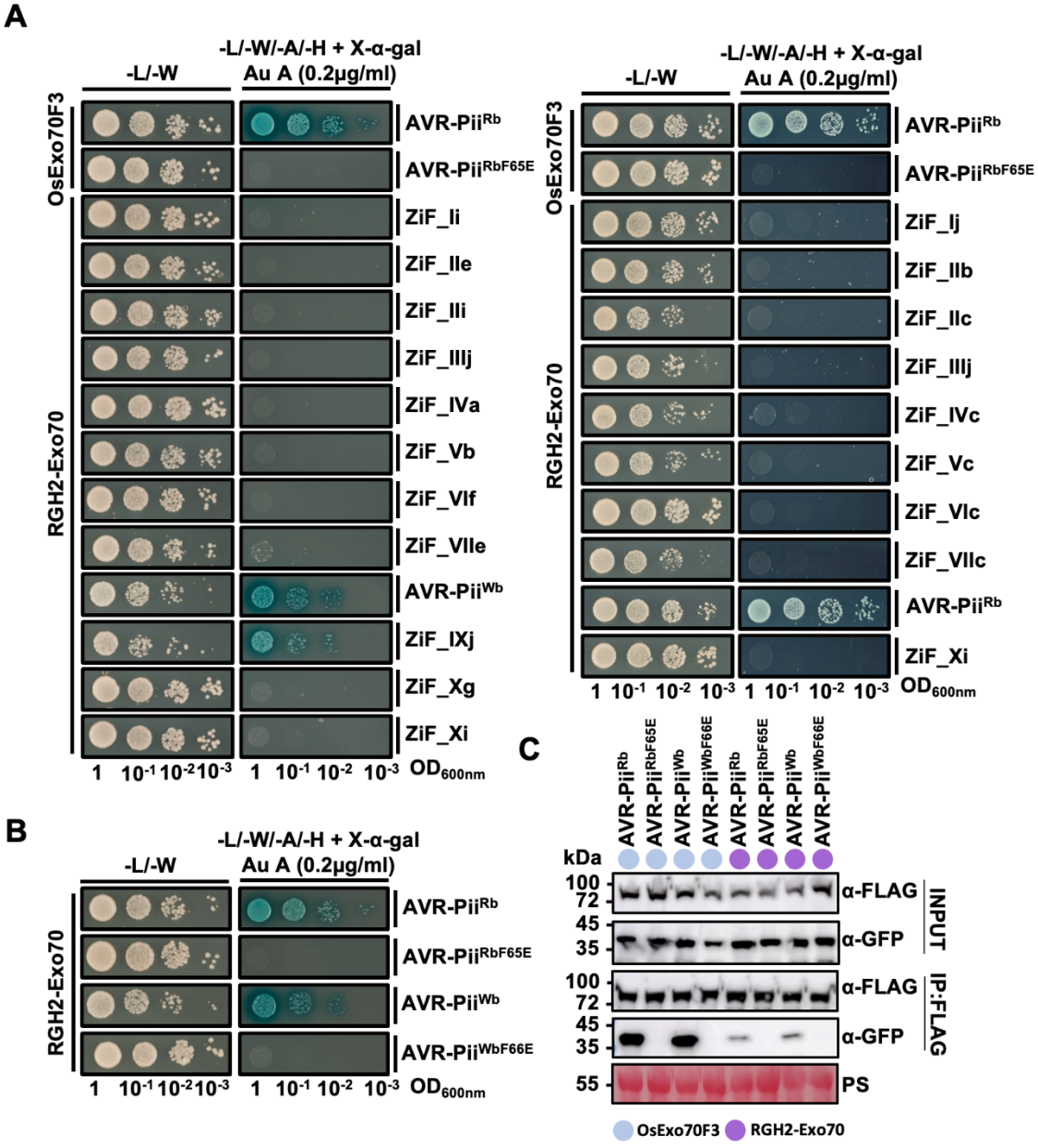
A
-L/-W
-L/-W/-A/-H + X-α-gal
Au A (0.2μg/ml)
OsExo70F3
RGH2-Exo70
AVR-Pii^Rb
AVR-Pii^RbF65E
ZiF_Ii
ZiF_IIe
ZiF_IIi
ZiF_IIIj
ZiF_IVa
ZiF_Vb
ZiF_VIf
ZiF_VIIe
AVR-Pii^Wb
ZiF_IXj
ZiF_Xg
ZiF_Xi
1 10^-1 10^-2 10^-3 OD600nm
ZiF_Ij
ZiF_IIb
ZiF_IIc
ZiF_IIIj
ZiF_IVc
ZiF_Vc
ZiF_VIc
ZiF_VIIc
B
AVR-Pii^WbF66E
C
AVR-Pii^Rb
AVR-Pii^RbF65E
AVR-Pii^Wb
AVR-Pii^WbF66E
kDa
100
72
45
35
55
α-FLAG
α-GFP
PS
INPUT
IP:FLAG
OsExo70F3
RGH2-Exo70
D
RGH2-Exo70
Time (mins)
Power (μcal/s)
ΔQ (kcal/mol of effector)
Δ(Fit-Exp)
Molar Ratio
K_d=1.5x10^-5M
K_d=N/A
K_d=6.7x10^-6M
K_d=N/A

968

969 **Figure 2: RGH2 interacts with rice blast AVR-Pii and the wheat blast variant in**
970 **vitro and in vivo.**

971 **A.** Y2H binding assay of the most prevalent ZiF effectors from wheat (left) and rice
972 (right) blast isolates as previously defined[32] to the RGH2-Exo70 integrated domain.
973 Yeast cells transformed with both plasmids were spotted onto selective synthetic
974 dropout (SD) media. For plates with quadruple-dropout media X-α-Gal and
975 Aureobasidin A (Au A) were added to the media. Yeast growth was monitored for
976 four days after plating. Growth and development of blue coloration indicates protein-
977 protein interactions. The experiment was repeated three times with comparable
978 results.

979 **B.** Interaction of rice blast AVR-Pii, the wheat blast variant and mutants with RGH2-
980 Exo70 using the Y2H assay. The experiment was carried out as described for panel
981 A. Yeast growth was monitored for four days subsequent to plating. The experiment
982 was repeated a minimum of three times, with similar results.

983 **C.** Co-IP assay showing that rice blast AVR-Pii and the wheat blast variant interact
984 with RGH2-Exo70-FLAG in *N. benthamiana.* The co-IP assays used an anti-FLAG
985 antibody to pull down AVR-Pii variants. Immunoblot analysis using an anti-GFP
986 antibody shows that RGH2-Exo70-FLAG and OsExo70F3-FLAG co-purified with rice
987 and wheat blast GFP-AVR-Pii variants but not with the effector mutants. Ponceau S
988 staining shows the total amount of protein loaded per lane in the input. The experiment
989 was repeated three times with similar results.

990 **D.** Binding of AVR-Pii variants to RGH2-Exo70 in vitro, as determined by ITC. Upper
991 panel shows the heat differences upon injection of AVR-Pii variants and mutants into
992 the cell containing RGH2-Exo70. Middle panel shows the integrated heats of injection
993 (dots-black colour) and best fit (solid line-magenta colour) to a single-site binding
994 model calculated using AFFINImeter ITC analysis software[68]. Bottom panel indicates
995 the difference between the fit to a single-site binding model and the experimental data.
996 The experiments shown are representative of three replicates.

997

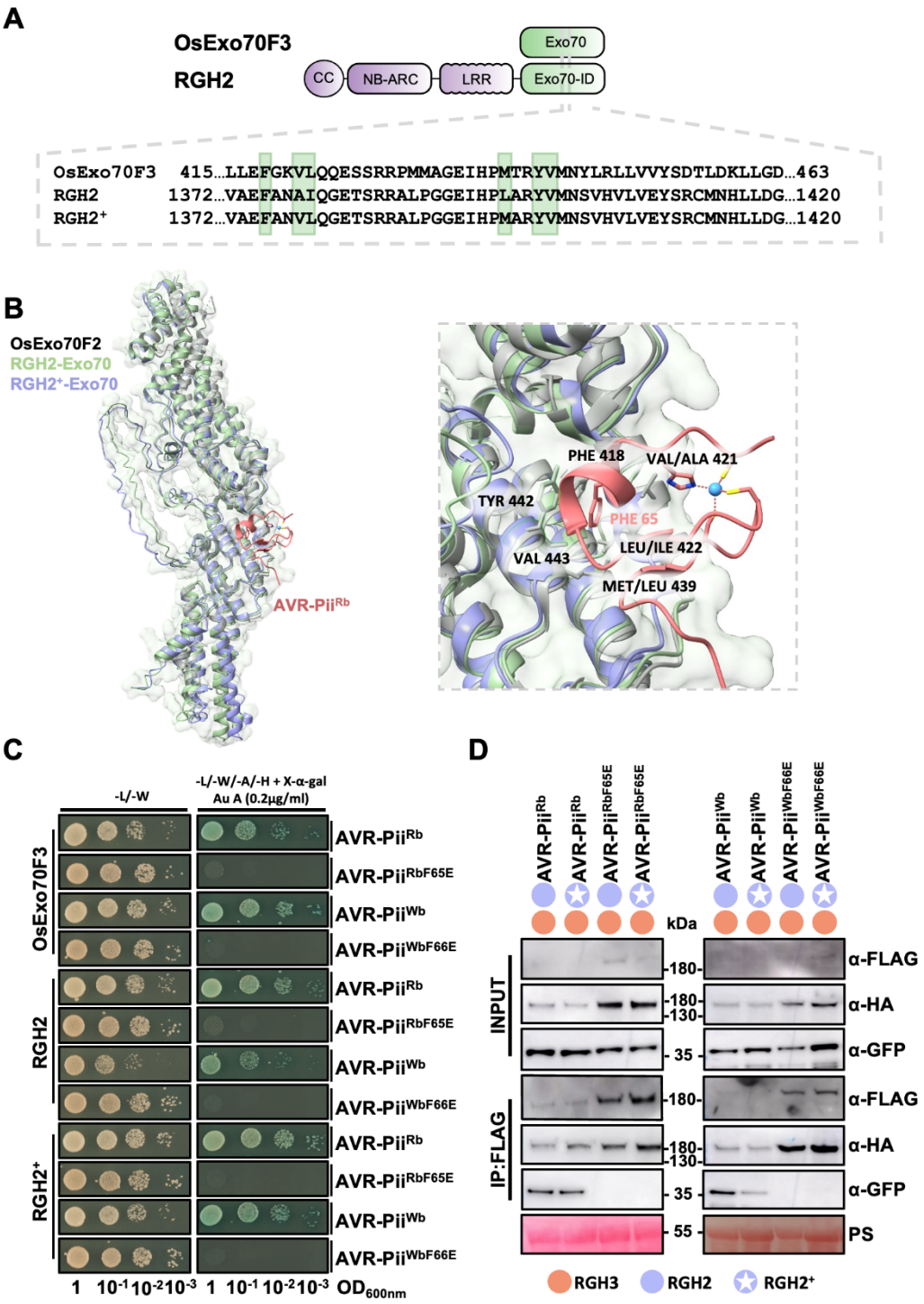

Figure 3: RGH2⁺ shows increased binding towards rice blast AVR-Pii and the wheat blast variant compared to RGH2.

A. Graphical representation of OsExo70F3 and the barley NLR RGH2. Sequence alignment of residues located at the effector binding interface in the OsExo70F2/AVR-Pii complex[29]. Residues important for the formation of the effector binding pocket are

1005 highlighted in green. To generate the engineered NLR RGH2^{+}, amino acid mutations
1006 Ala1378Val, Ile1379Leu, and Leu1396Met were made.

1007 **B.** Left, Structural predictions generated with AlphaFold3 as used to interpret
1008 interactions between AVR-Pii^{Rb} and RGH2-Exo70/RGH2^{+}-Exo70. The structure of
1009 OsExo70F2 in complex with AVR-Pii^{Rb} (PDB:7pp2) was previously determined[29].
1010 Right, zoom-in view of the binding interface in the OsExo70F2/AVR-Pii^{Rb} complex, with
1011 RGH2-Exo70 and RGH2^{+}-Exo70 superimposed. The residues of OsExo70F2 involved
1012 in binding the effector that are mutated in this study are indicated (Figure 3A). The
1013 AVR-Pii effector is shown in peach colour, with the Phe65 residue highlighted.

1014 **C.** Y2H assay of rice blast AVR-Pii, the wheat blast variant, and mutants with
1015 OsExo70F3, barley RGH2-Exo70 and RGH2^{+}-Exo70. Left, control plate for yeast
1016 growth; right, the quadruple-dropout medium supplemented with X-α-Gal and
1017 Aureobasidin A (Au A). The presence of yeast growth and the development of blue
1018 coloration in the selection plate signify positive protein-protein interactions. Yeast
1019 growth was monitored four days after plating. Each experiment was repeated at least
1020 three times, with consistent results obtained.

1021 **D.** Co-IP assay showing that rice blast AVR-Pii, and the wheat blast variant, interact
1022 with full length RGH2 and RGH2^{+} co-expressed with the helper NLR RGH3 in *N.*
1023 *benthamiana.* Co-IP assays were performed using an anti-FLAG antibody to pull down
1024 RGH2-FLAG and RGH2^{+}-FLAG interacting proteins. Immunoblot analysis using an
1025 anti-GFP antibody showed that GFP-AVR-Pii variants were pulled down with FLAG-
1026 RGH2 and FLAG-RGH2^{+}, but mutant effectors showed no interaction. Anti-HA was
1027 used to confirm the presence of RGH3-HA and interaction with RGH2. RGH2 and
1028 RGH2^{+} were only detected weakly in the inputs, but immunoprecipitated proteins are
1029 clear. Ponceau S staining shows the amount of total protein loaded per lane in the
1030 input. An expanded blot with additional controls is shown in Figure S9. Experiment
1031 was repeated at least three times, with similar results obtained.

1032

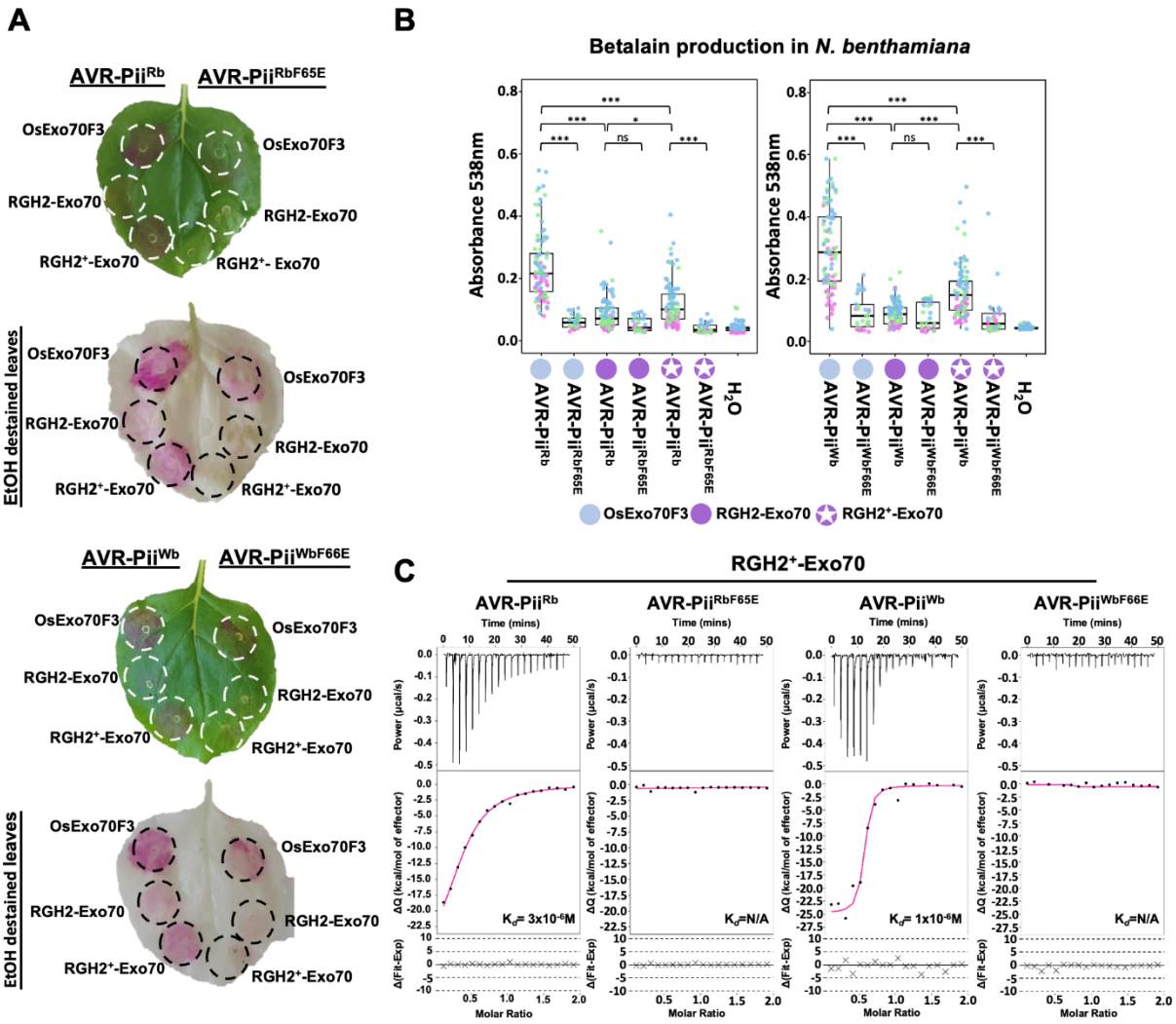

Figure 4: AVR-Pii^{Wb} exhibits increased binding to RGH2^{+} compared with RGH2 in planta and in vitro.

A. Betalain production in *N. benthamiana* leaves following Agrobacterium infiltration with OsExo70F3-GAL4-BD, RGH2-Exo70-GAL4-BD or RGH2^{+}-Exo70-GAL4-BD and rice or wheat blast VP16-GAL4-AD-AVR-Pii variants or mutant effectors. Leaves expressing RGH2^{+} show increased betalain accumulation compared to RGH2 with AVR-Pii variants. Upper panels show brightfield images of *N. benthamiana* leaves three days post infiltration. Lower panel shows the same leaves cleared overnight in 100% ethanol. Infiltration points are marked with a white or black circle.

B. Leaves cleared with ethanol were used for betalain extraction. The absorbance for betalain production was measured at OD_{538nm} from independent infiltration sites for each construct combination. Replicates are designated with different colours (magenta-Replicate 1 (R1), green-Replicate 2 (R2), blue-Replicate 3 (R3)). Box plots

1048 represent the median (horizontal line), upper and lower quartiles (boxes), and 1.5×
1049 interquartile range (whiskers). Asterisks indicate statistically significant differences
1050 from the control (NS: not significant, *$p < 0.05$, **$p < 0.01$, ***$p < 0.001$, one-way
1051 ANOVA followed by Tukey's test). Data shown are from a pool of three biological
1052 replicates, n = 15 plants per pool (30 infiltration points per one biological replicate).

1053 **C.** Binding of rice blast AVR-Pii, the wheat blast variant, and mutants to RGH2^{+}-Exo70
1054 in vitro, as determined by ITC. Upper panel represents the heat differences upon
1055 injection of effector variants and mutants into the cell containing RGH2^{+}-Exo70. Middle
1056 panel shows the integrated heats of injection (dots - black colour) and best fit (solid
1057 line - magenta colour) to a single-site binding model calculated using AFFINImeter ITC
1058 analysis software[68]. Bottom panel indicates the difference between the fit to a single-
1059 site binding model and the experimental data. The experiments shown are
1060 representative of three replicates.

1061

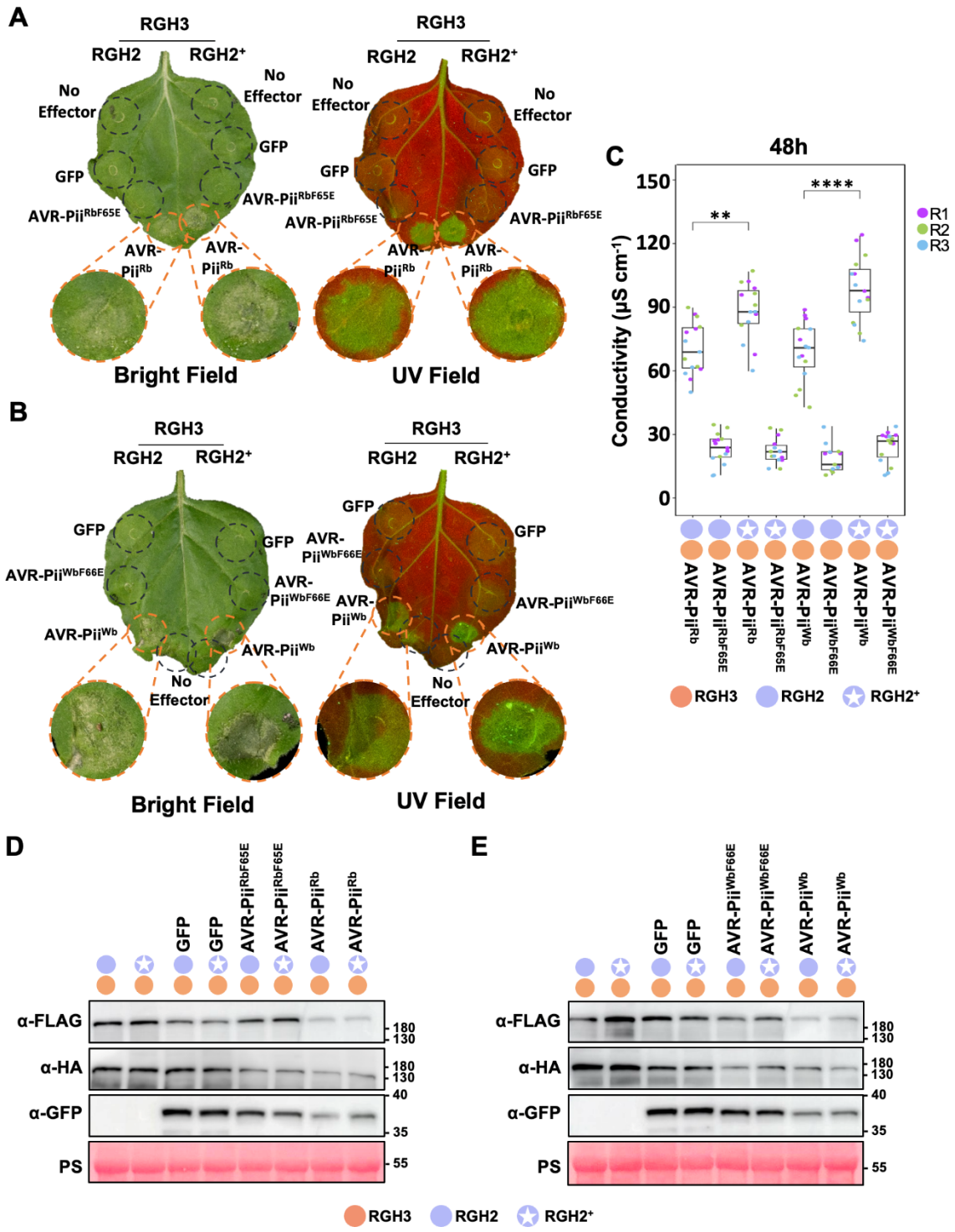

Figure 5: RGH2⁺/RGH3 elicit an increased cell death response to rice blast AVR-Pii and the wheat blast variant compared to RGH2/RGH3.

A. Macroscopic cell death phenotypes observed on transient expression of RGH2/RGH3 or RGH2⁺/RGH3 NLR pairs with GFP, GFP-AVR-Pii^{Rb} or GFP-AVR-

1068 Pii^{RbF65E} mutant in *N. benthamiana*. Leaves were photographed five days post
1069 infiltration and are representative of three independent experiments.

1070 **B.** As for Figure 5A but with the AVR-Pii^{Wb} variant and AVR-Pii^{WbF66E} mutant.

1071 **C.** Conductivity assay from *N. benthamiana* tissue infiltrated with RGH2/RGH3 or
1072 RGH2^{+}/RGH3 NLR pairs with rice or wheat blast GFP-AVR-Pii variants or mutants at
1073 48 hours post infiltration (hpi). Measurements of ion leakage after 4 and 24 hpi are
1074 shown in Figure S12. Box plots represent the median (horizontal line), upper and lower
1075 quartiles (boxes), and 1.5× interquartile range (whiskers). Statistically significant
1076 differences are denoted by an asterisk (NS: not significant, $^{**}p < 0.01$, $^{****}p < 0.0001$
1077 Student's t-test). Data from three independent experimental replicates are shown (n=5
1078 plants per experiment). Replicates are designated with different colours (magenta-
1079 Replicate 1 (R1), green- Replicate 2 (R2), blue-Replicate 3 (R3)).

1080 **D.** Expression of constructs used for the cell death and conductivity assays in *N.*
1081 *benthamiama* probed by western blot. RGH2-Exo70-FLAG, RGH2^{+}-Exo70-FLAG,
1082 RGH3-HA, the rice blast effector and AVR-Pii^{RbF65E} mutant were detected with the
1083 appropriate antibodies as labelled. Ponceau S staining shows the amount of total
1084 protein loaded per lane in the input.

1085 **E.** As for Figure 5D but with the AVR-Pii^{Wb} variant and AVR-Pii^{WbF66E} mutant.

1086

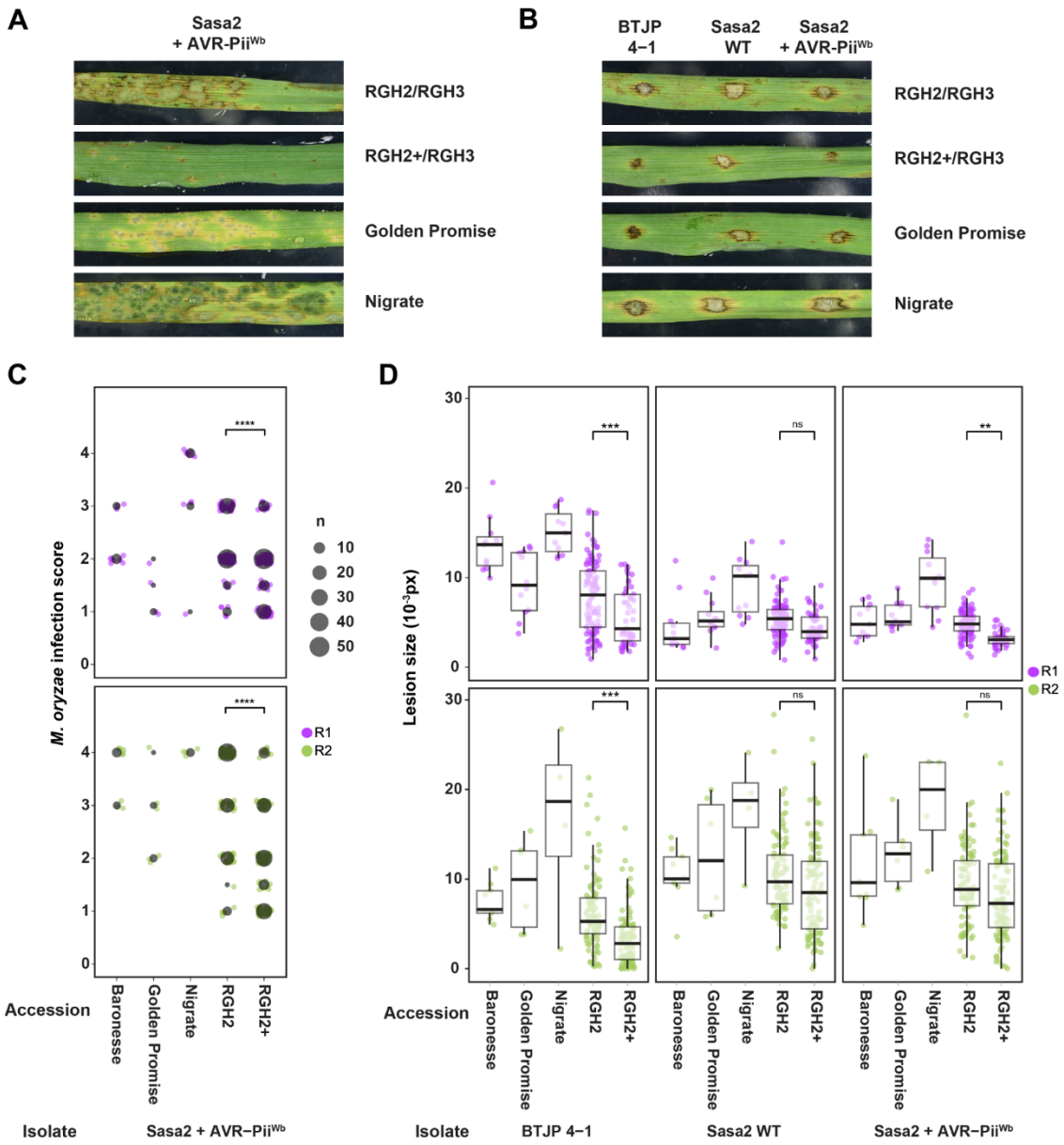

Figure 6: RGH2⁺/RGH3 transgenic lines show reduced virulence of *M. oryzae* isolates carrying AVR-Pii^{Wb}.

A. Macroscopic images of spray inoculations of disease phenotypes on barley accessions with transgenic *M. oryzae* isolate Sasa2 with AVR-Pii^{Wb}. Infections of individuals from T1 families of RGH2 and RGH2^{+} transgenics, Golden Promise transgenic background, and susceptible control Nigrate are shown.

B. Macroscopic images of spot inoculations of disease phenotypes on barley accessions with *M. oryzae* isolates BTJP 4-1, Sasa2 wild-type, and transgenic Sasa2 with AVR-Pii^{Wb}. Infection of individuals from T1 families of RGH2 and RGH2^{+}

1098 transgenics, Golden Promise transgenic background, and susceptible control Nigrate
1099 are shown.

1100 **C.** Box plots of lesion area of *M. oryzae* infection in spray inoculations of barley
1101 accessions with transgenic *M. oryzae* isolate Sasa2 transformed with AVR-Pii^{Wb}.
1102 Infection of individuals from T1 families of RGH2 and RGH2^{+} transgenics are plotted,
1103 alongside wild-type Baronesse (RGH2-RGH3), Golden Promise transgenic
1104 background, and susceptible control Nigrate. Asterisks indicate statistically significant
1105 differences between RGH2 and RGH2^{+} transgenics (****$p < 0.0001$, one-way ANOVA
1106 followed by Tukey's test). Data from two independent experimental replicates are
1107 presented with replicates designated with different colours (magenta-Replicate 1 (R1)
1108 and green- Replicate 2 (R2)).

1109 **D.** Box plots of lesion area of *M. oryzae* infection in spot inoculations of barley
1110 accessions with *M. oryzae* isolates BTJP 4-1, Sasa2 wild-type, and transgenic Sasa2
1111 with AVR-Pii^{Wb}. Infection of individuals from T1 families of RGH2 and RGH2^{+}
1112 transgenics are plotted, alongside wild-type Baronesse (RGH2-RGH3), Golden
1113 Promise transgenic background, and susceptible control Nigrate. Asterisks indicate
1114 statistically significant differences between RGH2 and RGH2+ transgenics
1115 (***$p < 0.001$, **$p < 0.01$, one-way ANOVA followed by Tukey's test). Data from two
1116 independent experimental replicates are presented with replicates designated with
1117 different colours (magenta-Replicate 1 (R1) and green- Replicate 2 (R2)).

1118